Article

Real Time Fault Location Using the Retardation Method

Moneer Nabwani [1,2,†], **Michael Suleymanov** [1,†], **Yosef Pinhasi**[1,†] **and Asher Yahalom** [1,3,†]* ⓘD

1   Department of Electrical & Electronic Engineering, Ariel University, Kiriat Hamata POB 3, Ariel 40700, Israel;
2   Israel Electric Company (IEC), Netiv Haor 1, POB 10, Haifa 3100001, Israel;
3   Princeton University, Princeton, New Jersey 08543, USA;
*   Correspondence: asya@ariel.ac.il;
†   These authors contributed equally to this work.

Abstract: A new method for short circuit fault location is proposed based on instantaneous signal measurement and its derivatives, and is based on the retardation phenomena. The difference between the times in which a signal is registered in two detectors is used to locate the fault. Although a description of faults in terms of a lumped circuit is useful for elucidating the methods for detecting the fault. This description will not suffice to describe the fault signal propagation hence a distributed models is needed which is given in terms of the telegraph equations. Those equations are used to derive a transmission line transfer function, and an exact analytical description of the short circuit signal propagating in the transmission line is obtained. The analytical solution was verified both by numerical simulations and experimentally.

1. Introduction

One of the most important results of special relativity is the fact that no signal can travel faster than the speed of light in vacuum c [1]. The same is true for a signal generated from a fault occurring in a power transmission line such as short or a disconnection. As the signal due to the fault reaches detectors along the line at different times (due to finite propagation speed), one can use the differences in the time of arrival to locate the fault along the line. This location technique is passive in the sense that one does not need to inject any signal to the power line in order to locate the fault, rather the fault itself is the source of the signal. Another advantage is that the detection and location are done in real time. Still several issues are raised regarding the proposed technique:

- What is the signal velocity, and what is the needed sampling rate?
- What should be measured (voltage and/or current)?
- How many detectors are needed?
- What are the dispersion effects on the prorogation of the signal and how do they effect accuracy?
- What are the best practices for signal processing in order to obtain an accurate time of arrival.
- How does the current technique compare in terms of accuracy with previous art?

We will try to answer those questions in the current paper. The discussion will be limited to low voltage transmission lines while the discussion of high voltage transmission lines will be the subject of a future paper.

Power transmission lines have a broad range of faults. These fault classifications appear in various previous articles [2–9]. There are several approaches to fault location algorithms, including various approaches regarding measurements and data processing and their proposed applications. A bridge circuit method [10] employs an adjustable impedance to calculate the location of the fault. M. N. Alam et al. [11] present a method based on surface electromagnetic waves propagating along a transmission line. In M. Aldeen and F. Crusca's study [12], the faults are modelled as unknown inputs, decoupled

from the state and output measurements through coordinate transformations, and then estimated via the use of the observer theory. The article by Qais Alsafasfeh et al. [13] presents a method that integrates the symmetrical components technique with principal component analysis (PCA) for fault classification and detection. In another research [14], Petri nets were used to obtain the modeling and location detection of faults in power systems. Another widely used method is that of wavelet transform analysis [15–18]. We will compare the accuracy of the current method to the accuracy of previous art in the concluding section.

The plan of the paper is as follows: First we present the basic idea of the method. Then we provide a description of the fault in terms of a lumped circuit which is useful for elucidating the methods for detecting the fault, here we shall demonstrate the ability to determine the signal arrival time using derivatives. This description will not suffice, however, to describe the fault signal propagation hence a distributed models is needed which will be given in terms of the telegraph equations [19–22]. After introducing the main formalism and the telegraph equations of the distributed system we take a specific example of a two-wire power line. We will present several models to describe the development of a short and the signal generated in a possible detector due to that short. Those will include exponential, Gaussian and step function forms. For the step function model an inverse Laplace transform will allow us to determine the time dependent signal at the sensor position analytically. At this stage we will compare the analytical and numerical solutions. Next the experimental setup will be described. We will show a high level of conformity of the theoretical and experimental measurements using the appropriate data processing. Finally,we shall determine the system accuracy and compare it with previous methods.

2. Fault detection by retardation

Consider a fault of unknown location which causes a signal propagating to both sided of the transmission line (see figure 1). The signal is registered by a detector which determines its time of arrival, t_1 for detector 1 and t_2 for detector 2.
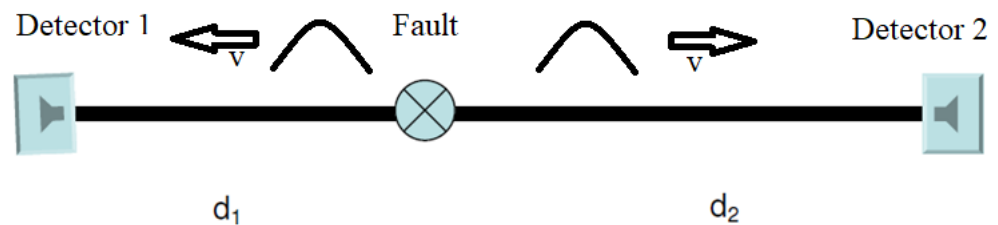

Figure 1. Transmission line with a short and detectors

If the unknown time in which the fault occurred is t_0 and the constant velocity of signal propagation is v the following relations follow:

$$v(t_1 - t_0) = d_1; \qquad v(t_2 - t_0) = d_2 \qquad (1)$$

In which d_1 and d_2 are the unknown distance from the fault to detectors 1 and 2 respectively. The total distance between the two detectors is known as:

$$d = d_1 + d_2 \qquad (2)$$

Defining the time difference $t_{di} \equiv t_2 - t_1$, the distance from detector 1 to the short may be written as follows:

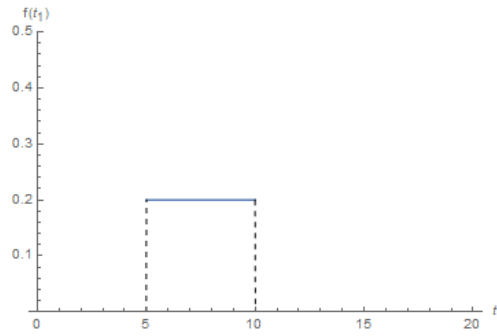$$d_1 = \frac{1}{2}(d - v\,t_{di}) \qquad (3)$$

Figure 2. Uniform distribution probability density function of t_1, in the illustration we assume $T = 5$ and $t_D = 10$.

Hence if t_{di} is a random variable of standard deviation $\sigma_{t_{di}}$, the corresponding standard deviation of d_1 is:

$$\sigma_{d_1} = \frac{v}{2}\sigma_{t_{di}} \qquad (4)$$

provided we assume that the velocity v is known. Now $\sigma_{t_{di}}$ can be evaluated as:

$$\sigma_{t_{di}} = \sqrt{\sigma_{t_1}^2 + \sigma_{t_2}^2 - 2C_{t_1 t_2}}. \qquad (5)$$

In which the covariance $C_{t_1 t_2}$ is given in terms of the following expectation value:

$$C_{t_1 t_2} = E[(t_1 - \bar{t}_1)(t_2 - \bar{t}_2)], \qquad \bar{t} \equiv E[t] \qquad (6)$$

If the uncertainty in t_1 is uncorrelated to the uncertainty in t_2 the covariance is null and we have a simplified expression:

$$\sigma_{t_{di}} = \sqrt{\sigma_{t_1}^2 + \sigma_{t_2}^2}. \qquad (7)$$

If $\sigma_{t_1} = \sigma_{t_2}$ this will result in:

$$\sigma_{t_{di}} = \sqrt{2}\sigma_{t_1}. \qquad (8)$$

Thus, we can rewrite σ_{d_1} in terms of σ_{t_1} as follows:

$$\sigma_{d_1} = \frac{v}{\sqrt{2}}\sigma_{t_1} \qquad (9)$$

Now suppose that the data is sampled at intervals of T, if the signal is detected initially at time t_D it means that the signal arrived at any time between t_D and $t_D - T$. Since we do not have any information in which time the signal has really arrived, we assume that t_1 is a random variable distributed uniformly in the interval $[t_D - T, t_D]$. The probability density function of t_1 is depicted in figure 2. Since the moments of a uniform distribution function are known, we can easily evaluate the expectation and standard deviation of t_1 as follows:

$$\bar{t}_1 = t_D - \frac{1}{2}T, \qquad \sigma_{t_1} = \frac{T}{2\sqrt{3}} \qquad (10)$$

Inserting the result of equation (10) into equation (9) will lead to:

$$\sigma_{d_1} = \frac{vT}{2\sqrt{6}} \qquad (11)$$

Thus the accuracy at which we need to know the location of the fault will determine the sampling rate f_S according to the following formula:

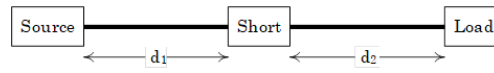$$f_S = \frac{1}{T} = \frac{v}{2\sqrt{6}\,\sigma_{d_1}} \qquad (12)$$
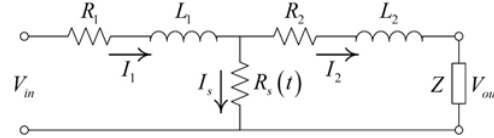
Figure 3. Transmission line with a short

Figure 4. Short circuit example

As we shall show later for a power line the typical propagation of the signal is close to lights velocity in vacuum:

$$v \simeq c \simeq 3 \ 10^8 \ \text{m/s}. \tag{13}$$

Thus, if the required distance precision is of about 1 meter, then the time measurement sampling rate should be:

$$f_S \simeq 6.12 \ 10^7 \text{Hz} \tag{14}$$

This is much lower than the clock rate of current computer processors. We will not deal here with additional sources of uncertainty such as the noise level of transmission lines and will leave that for future work.

3. Signal detection

What kind of signal should we measure for fault location, should it be voltage or current? And how should it processed in order to avoid accumulation of a large amount of unnecessary data due to the high sampling rate dictated by equation (14)? We shall try to answer those question using a lumped circuit model as follows [23–25].

3.1. The lumped circuit model

The schematic description of the short circuit is presented in Figure 3. This is modelled in figure 4 such that the parts of the transmission line before and after the short circuit as a resistor and inductor connected in a series. In order to mathematically analyse this we use the Kirchhoff voltage law and Ohm's law:

$$\begin{aligned}
V_{in}(t) &= R_1 I_1(t) + L_1 \frac{dI_1(t)}{dt} + V_S(t) \\
V_S(t) &= R_2 I_2(t) + L_2 \frac{dI_2(t)}{dt} + V_{out}(t) \\
V_{out}(t) &= Z I_2(t)
\end{aligned} \tag{15}$$

in which V_{in} is the source voltage, I_1 is the source current, V_S is the short voltage, I_2 is the load current, V_{out} is the load voltage. R_1 and L_1 are resistance and inductance before the short, R_2 and L_2 are resistance and inductance after the short and Z is the load impedance.

3.2. The case of resistive impedance

In the first step, we ignore the inductance for mathematical simplicity. We also notice that by Ohm's law:

$$V_S(t) = R_S(t) I_S(t) \tag{16}$$

where $R_S(t)$ is the time dependent short resistance, and $I_S(t)$ is the current flowing through the short. According to Kirchhoff's current law:
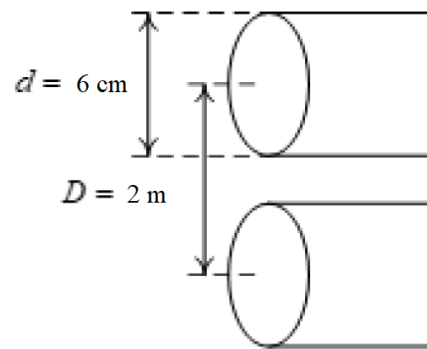
$$I_S(t) = I_1(t) - I_2(t) \tag{17}$$

Figure 5. Cable geometry for demonstration

Table 1. Two-wire cable parameters

Parameter	Value	Unit
σ_c(Copper)	$5.96 \cdot 10^7$	S/m
d	0.06	m
D	2	m
l	1000	m

Thus, the currents in this case can be calculated algebraically as follows:

$$I_1(t) = \frac{Z+R_2+R_S(t)}{R_1 \cdot [Z+R_2+R_S(t)]+R_S(t) \cdot (Z+R_2)} \cdot V_{in}(t)$$
$$I_2(t) = \frac{R_S(t)}{R_1 \cdot [Z+R_2+R_S(t)]+R_S(t) \cdot (Z+R_2)} \cdot V_{in}(t) \qquad (18)$$
$$I_S(t) = \frac{Z+R_2}{R_1 \cdot [Z+R_2+R_S(t)]+R_S(t) \cdot (Z+R_2)} \cdot V_{in}(t)$$

In the current model, the transmission line is a two-wire copper cable; each wire has a diameter d ,and the distance between them is D, the cable is depicted in figure 5. The total cable length is l. Values used for a demonstration are given in table 1. The surface resistance in ohm (Ω) may be written as follows [26]:

$$R_{Surface} = \sqrt{\frac{\omega \mu_c}{2\sigma_c}} = \sqrt{\frac{\pi f \mu_c}{\sigma_c}} \qquad (19)$$

in the above ω is the angular frequency, f is the frequency, μ_c is the magnetic permeability of the material and σ_c is the conductivity. Hence, the resistance per unit length $[\Omega/m]$ can be written as:
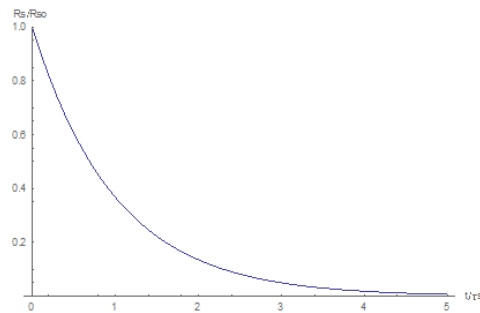
$$R = 2\frac{R_{surface}}{2\pi\frac{d}{2}} = 2\frac{R_{surface}}{\pi d} \qquad (20)$$

Table 2. Two-wire cable resistance

Parameter	Value	Unit
μ_c	$4\pi \cdot 10^{-7}$	H/m
f	50	Hz
$R_{surface} = \sqrt{\frac{\pi f \mu_c}{\sigma_c}}$	$1.82 \cdot 10^{-6}$	Ω
$R = 2\frac{R_{surface}}{\pi d}$	$1.93 \cdot 10^{-5}$	$\frac{\Omega}{m}$

Table 3. Short circuit parameters

Parameter	Value	Unit
l_1	300	m
$l_2 = l - l_1$	700	m
τ_S	100	Nano-Second
ρ_{S0} (Air)	$1.3 \cdot 10^{16}$	$\Omega\,m$
l_S	0.1	m
A_S	0.0004	m^2
$R_{S0} = \frac{\rho_{S0} l_S}{A_S}$	$3.25 \cdot 10^{18}$	Ω

Figure 6. Short circuit resistance

The values used for the cable description appear in table 2. We notice that the value of $f = 50$ Hz used above is typical for many power lines. However, as the typical duration of the short is miniscule the signal generated by the short will include a broad band of frequencies each suffering a different impedance. This will be dealt with in later part of this paper. However, here we assume for simplicity that the resistance is constant.

The short circuit appears at distance l_1 from the input. The short-circuit $R_S(t)$ resistance is shown in figure 5. The short is described by a time dependent resistance which is assumed to behave exponentially:

$$R_S(t) = R_{S0} e^{-\frac{t}{\tau_S}}. \tag{21}$$

The initial resistance $R_S(0) = R_{S0}$ is assumed to be very large and represents the region's air resistance. However, at time $t = 0$ a short is initiated causing an exponential decrease in the short resistance at a typical duration of $\tau_S = 10 - 100\,[ns]$ which depends on conditions and geometry of the short circuit region. The short circuit parameters are concentrated in Table 3. Thus the current flows through the short instead of the load causing a decrease in the load current. Moreover, since the overall impedance of the circuit is decreased and is now dominated by the impedance of the short the current at the source becomes much higher.

The transmission line resistances and the load impedance are described in table 4. The

Table 4. Transmission line resistance and the load impedance

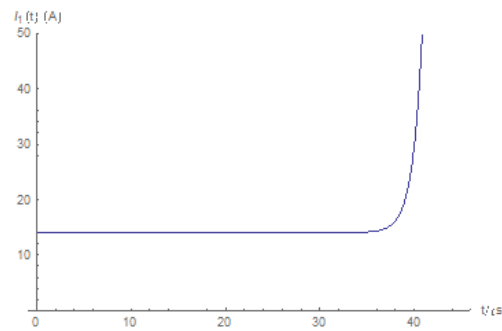| Parameter	Value	Unit
$R_1 = R \cdot l_1$	0.00579	Ω
$R_2 = R \cdot l_2$	0.0135	Ω
$R_T = R_1 + R_2$	0.0193095	Ω
Z	15.625	Ω

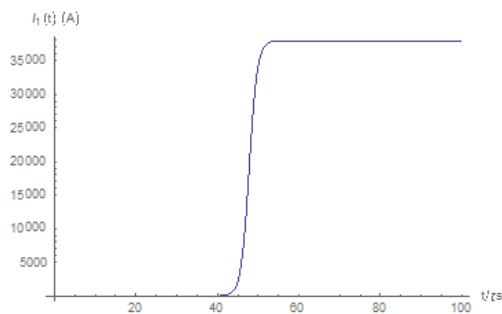**Figure 7.** Source current before the short

Figure 8. Source current after the short

input voltage is assumed to be of the form:

$$V_{in}(t) = A_0 \cos(\omega_0 t), \tag{22}$$

where $A_0 = 220\,[V]$, $\omega_0 = 2\pi f_0 = 100\pi\,[rad/s]$. We shall now present the calculation results.

3.2.1. Current

The source current just before the short is depicted in figure 7 and after the short is depicted in figure 8.

Hence the current at the source is a highly sensitive indicator for the occurrence of a short. To avoid storing unnecessary data and for precise timing of the short occurrence one can look at the source current derivative (figure 9) this has a distinctive pulse shape. Hence by taking the derivative of the signal and by fixing a high detection threshold one can avoid recording unnecessary data. On the load side, the current vanishes after the short occurs (Figure 10), hence the load current is also an excellent indicator of the short occurrence.

Again we see that on the load side, the current behavior allows for identification of the short by taking the current derivative (figure 11). This method allows precise timing with the need to store a small amount of data as indicated above.
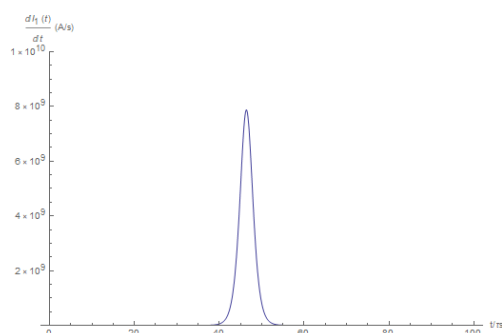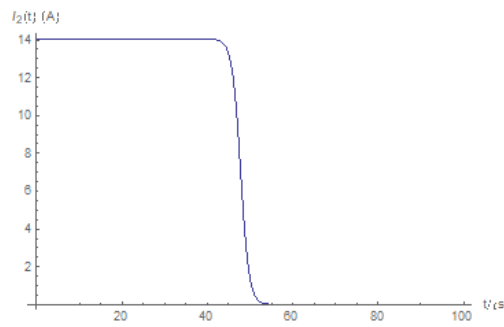

Figure 9. Source current derivative.
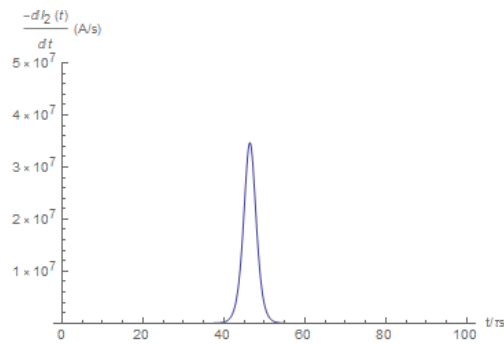
Figure 10. Load current

Figure 11. Load current derivative

3.2.2. Voltage

The short circuit pulse may also be detected by voltage measurement. For example, the voltage measured at half a distance between the source and the short will yield a voltage V_1 as follows:

$$V_1(t) = V_{in}(t) - \frac{1}{2}R_1 I_1(t) \tag{23}$$

This voltage is depicted in figure 12.

Again the distinctive pulse shape of the voltage derivative (figure 13) is apparent with the same advantage mentioned before.

The voltage at the short vanishes (figure 14), since the resistance approaches zero during the short creation, providing the same behavior that allows the pulse form in the voltage derivative (figure 15). Similarly, the voltage V_2 at half a distance between the short and the load may be measured (figure 16) and the pulse may be detected using the voltage derivative (figure 17).

$$V_2(t) = V_s(t) - \frac{1}{2}R_2 I_2(t) \tag{24}$$

Summarizing the results of our first model, we saw that the current and voltage measurements enable the short pulse detection, indicating the short occurrence. Likewise, it was
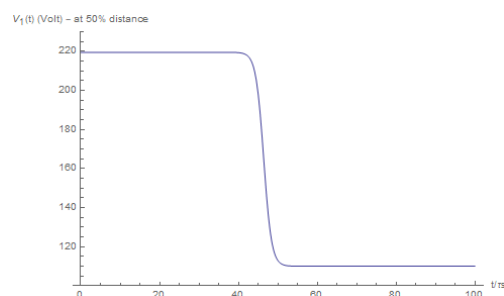

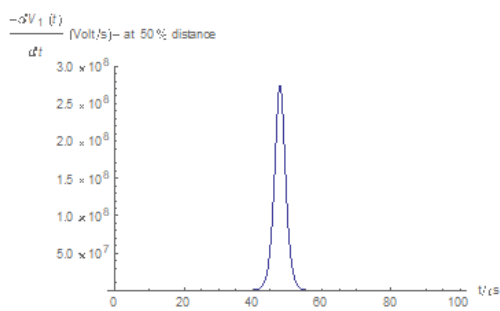**Figure 12.** Voltage at half the distance between the source and the short

Figure 13. Voltage derivative at half the distance between the source and the short
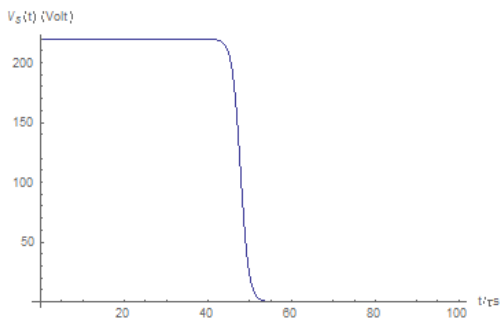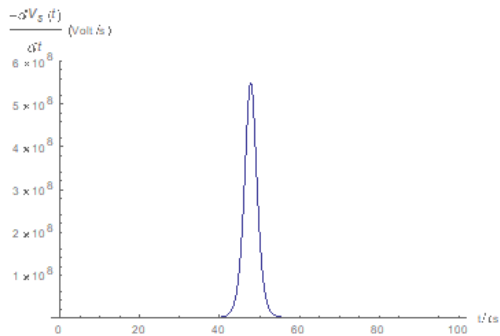

Figure 14. Voltage at the short

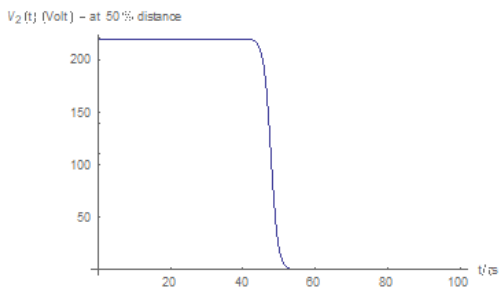**Figure 15.** Voltage derivative at the short

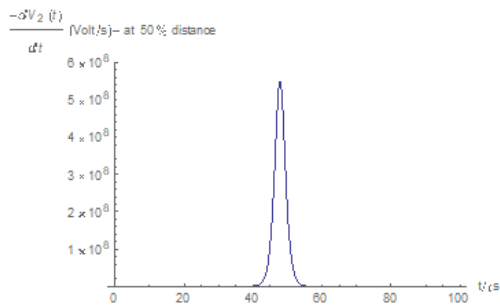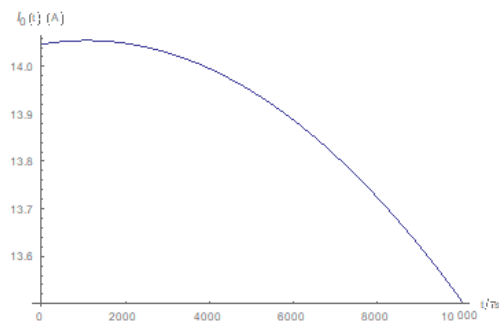**Figure 16.** Voltage at half the distance between the short and the load

Figure 17. Voltage derivative at half the distance between the short and the load

Table 5. Transmission line inductance

Parameter	Value	Unit
$L = \frac{\mu}{\pi} ar \cosh\left(\frac{D}{d}\right)$	$1.68 \cdot 10^{-6}$	$\frac{H}{m}$
$L_1 = L \cdot l_1$	0.000503938	H
$L_2 = L \cdot l_2$	0.00117585	H
$L_T = L_1 + L_2$	0.00167979	H

Figure 18. The initial current

shown that detection is possible both on the source and the load side. In order to detect the pulse, a resolution of the τ_S order is needed. In the current model, the inductance is neglected leading to a simplified description, in the next section we will look at the case were induction is taken into account leading to somewhat more complex mathematical analysis. Moreover, in a lumped model there is no pulse propagation along the transmission line and for this purpose we will introduce a distributed model later in this paper.

3.3. The case of resistive and inductive impedance

In this model, the transmission line inductance is no longer neglected as in previous section. Therefore, the equations given in (15) become coupled differential equations that can only be solved numerically. The two-wire cable induction can be calculated and is shown in Table 5. The current in the circuit before the short occurs can be calculated analytically and is given, as follows:

$$I_{10}(t) = I_{20}(t) = \frac{A_0 \cdot A_t}{Z + R_T} \cdot \cos[\omega \cdot t + \varphi_t] \qquad (25)$$

where: $A_t \equiv \dfrac{1}{\sqrt{1+\left(\omega \cdot \tau_p\right)^2}}$, $\varphi_t \equiv -\arctan[\omega \cdot \tau_p]$,

$\tau_p \equiv \frac{L_T}{Z}$. This current is depicted in figure 18. We will now study the numerical solutions of equation (15) given the above initial form.

3.3.1. The current

The source current is demonstrated in figures 19 (right after the short) and 20 (a long time after the short). In the previous model, the derivative had a pulse shape. In the current model, the first derivative does not exhibit a pulse shape (figure 21), however, the second derivative (figure 22) does exhibit a pulse shape with all the benefits mentioned previously. Current measurements on the load side also provide the short pulse detection ability. The load current is shown in figures 23 (right after the short) and 24 (a long time after the short). Here the current decay is evident. The current's first and second derivatives are shown in figures 25 and 26, respectively. We see that the short may be detected and accurately timed by the current's second derivative, measured on either the source or the load side. Next, we investigate the current at the short itself. It is obvious that it is zero before the
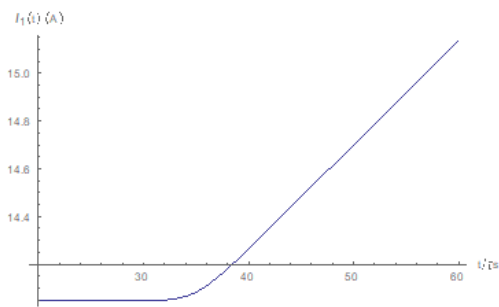
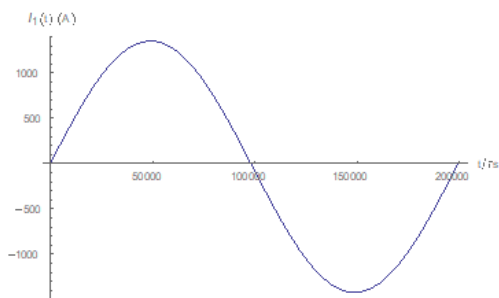**Figure 19.** Source current right after the short

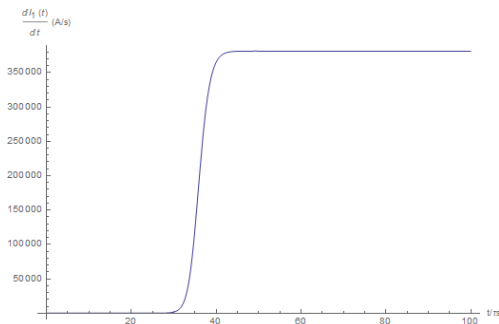**Figure 20.** Source current long time after the short

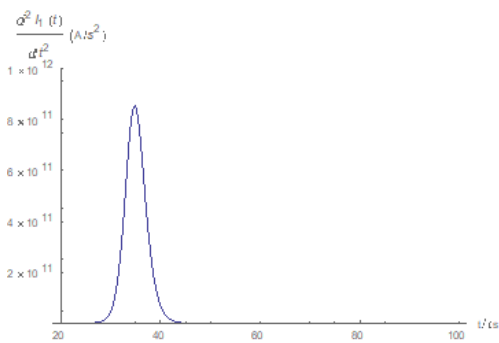**Figure 21.** The source current derivative.

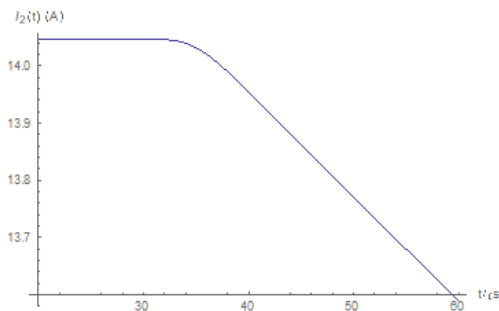**Figure 22.** The source current second derivative

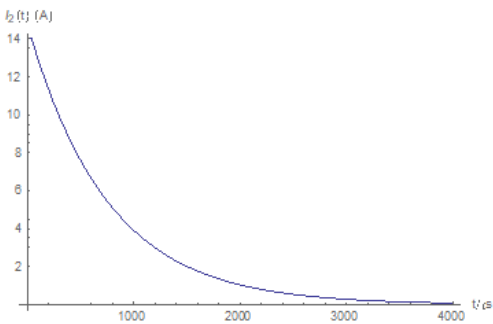**Figure 23.** Load current (right after the short)

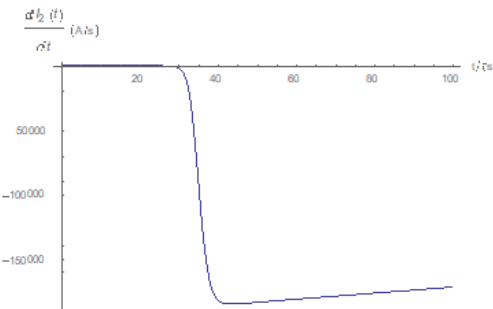**Figure 24.** Load current (after some time)

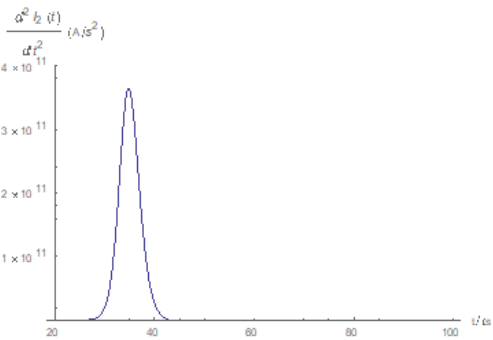**Figure 25.** The load current derivative

Figure 26. The load current second derivative
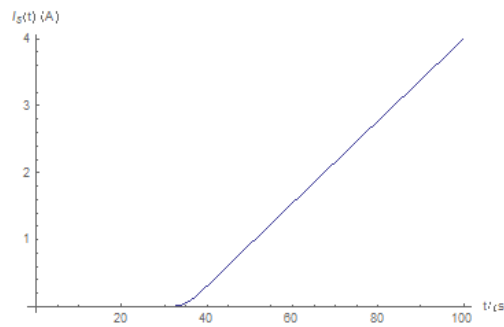
Figure 27. Short current (right after the short)
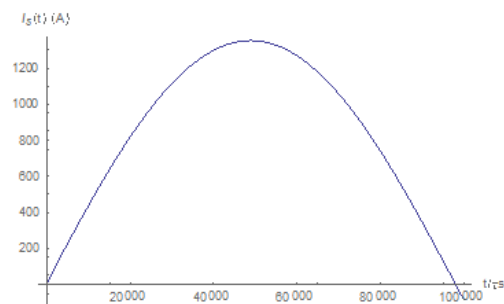
Figure 28. Steady state short current

short happens, after which it grows linearly (figure 27). After some time, the short current reaches the characteristic source current values (figure 28).

3.3.2. The voltage

The short-circuit pulse may also be detected by voltage measurement between the source and the short. If the voltage is measured at half a distance, due to a high short current, the voltage will be:

$$V_1(t) = V_{in}(t) - \frac{1}{2}R_1 I_1(t) - \frac{1}{2}L_1 \frac{dI_1(t)}{dt} \tag{26}$$

The voltage and its derivative are shown in figures 29 and 30 respectively. We deduce that for the voltage case a first derivative will suffice for short location even when inductance is not neglected. Figure 31 and 32 describe the voltage and its derivative at the short itself. We see that the voltage difference on the short when its resistivity goes to zero is also zero, and the pulse behavior of the voltage derivative is depicted.

Figure 29. Voltage at half a distance between the source and the short
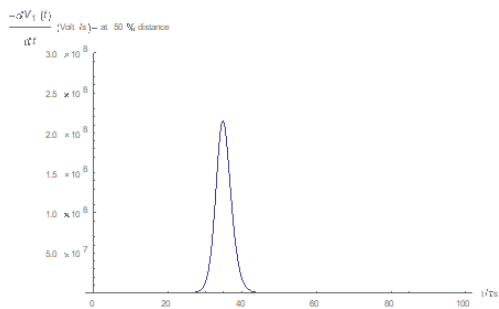
Figure 30. Voltage derivative at half a distance between the source and the short
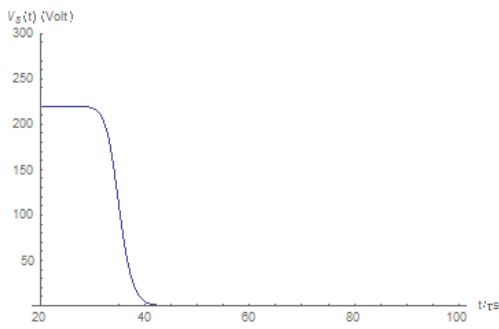
Figure 31. The short voltage
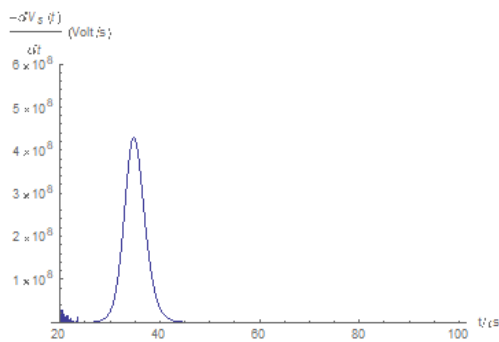
Figure 32. The short voltage derivative
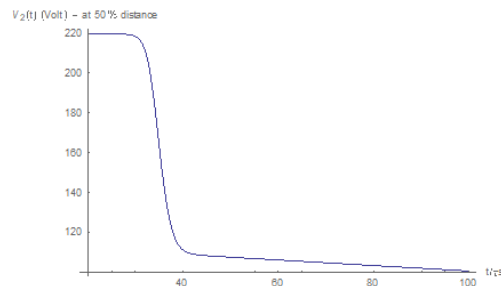
Figure 33. Voltage at half a distance between the short and the load (right after)
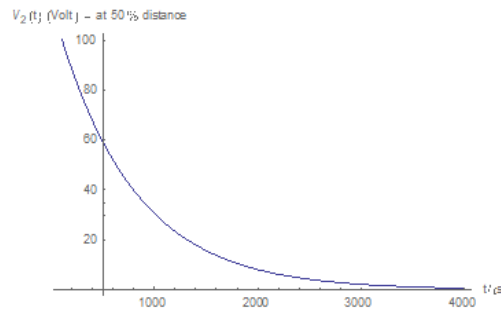
Figure 34. Voltage at half a distance between the short and the load (after some time)
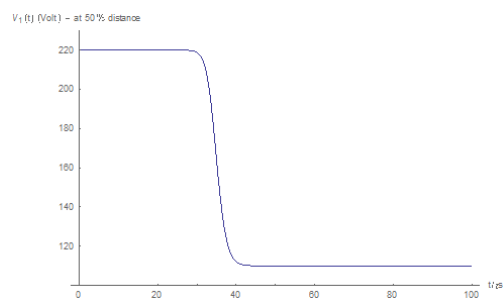
Analogous results may be obtained if the voltage is measured on the load side, even if the measurement is not on the load itself. For example, for half a distance voltage measurement, one obtains:

$$V_2(t) = V_s(t) - \frac{1}{2}R_2 I_2(t) - \frac{1}{2}L_2\frac{dI_2(t)}{dt} \qquad (27)$$

Figures 33 and 34 show the voltage at half a distance between the short and the load. The voltage in a brief duration after the short is formed is depicted in figure 33 and a longer duration of the same is depicted in figure 34.

The voltage derivative displays pulse behavior (figure 35) and thus in this case a first derivative will suffice and a second derivative is not needed. Finally, the load voltage is described, which is proportional to the load current (see also equation (15)):

$$V_{out}(t) = Z \cdot I_2(t) \qquad (28)$$

The load voltage, after a brief duration since the short occurrence and later, are shown in figures 36 and 37 respectively.

The first and the second load voltage derivatives are shown in figures 38 and 39. In this case the desirable pulse shape is attained for the second derivative.

Figure 35. Voltage derivative at half a distance between the short and the load

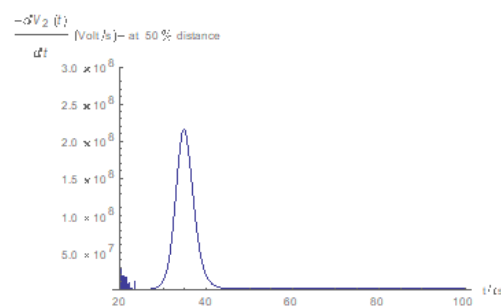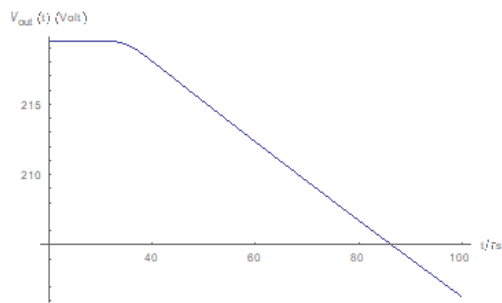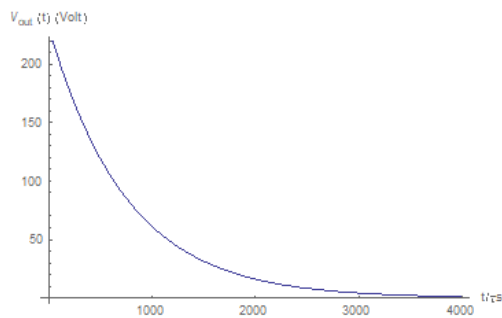**Figure 36.** Load voltage (right after the short)
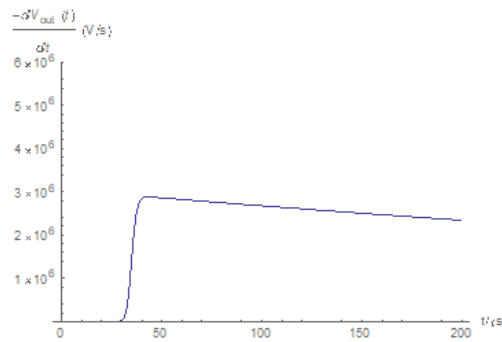

Figure 37. Load voltage (after some time)
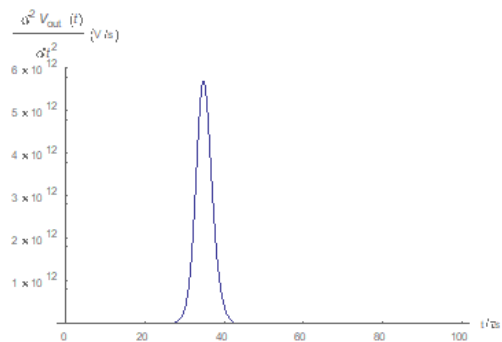

Figure 38. Load voltage derivative

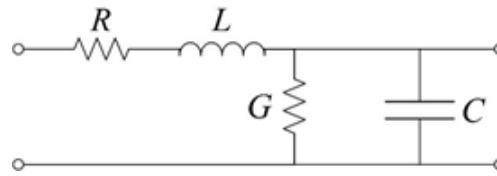**Figure 39.** Load voltage second derivative

Figure 40. Transmission line structure for a single unit length

3.4. Intermediate account

The high sampling rate which is needed for accurate location as described in equation (12) imposes a storage challenge as the amount of data accumulated may be prohibitive. However, taking the derivative of the signal which may be voltage or current allows us to over come this obstacle. By choosing a high detection threshold one avoids false positives and allows us to store a relatively small amount of data which is sufficient for detection and location of the short. In some cases a second derivative is required.

Generally, the first voltage derivative is enough (except for the load voltage), while in the case of current measurement the second derivative is necessary.

We further notice an additional restriction on the required resolution T, in order to avoid the case that the pulse goes undetected, that is between sampling points we need to have a resolution smaller than the pulse duration which is of the same duration as the time it takes the short to form, hence:

$$T < \tau_S \tag{29}$$

Now if $\tau_S \simeq 10^{-8}$ seconds this will mean that:

$$T < 10^{-8} \text{ seconds} \tag{30}$$

This limitation is even more restrictive than the one appearing in equation (14) leading to:

$$T_S = \frac{1}{f_S} \simeq 1.63 \, 10^{-8} \text{ seconds} \tag{31}$$

Obviously a lumped model neglects the effect of spatial distances and hence the effect of signal propagation. To describe the effect of signal propagation properly a distributed model is needed, in such a model we could study the short signal propagation and related phenomena such as dispersion, this is discussed in the following section.

4. Distributed Model

Until now, we have ignored the signal propagation in the circuit and assumed that the changes in the voltage and the current occur immediately and simultaneously everywhere. This assumption is not compatible with the theory of special relativity, which states that any signal must propagate with finite velocity, smaller than the speed of light in a vacuum [1]. To describe this behavior, we use the transmission-line propagation model [26], a section of which is depicted in figure 40.

This approach leads to the telegraph equations. We will describe this model in the time and frequency domains and draw the relevant conclusion from each presentation.

4.1. The time domain

The equations that describe the voltage and the current dependence in the time domain are the telegraphs equations given below [26]:

$$\frac{\partial V(x,t)}{\partial x} = -RI(x,t) - L\frac{\partial I(x,t)}{\partial t}$$
$$\frac{\partial I(x,t)}{\partial x} = -GV(x,t) - C\frac{\partial V(x,t)}{\partial t} \tag{32}$$

where R is the resistance, L is the inductance, G is the conductance and C is the capacitance, per unit length each (see figure 40). This pattern is repeated indefinitely (see figure 41).
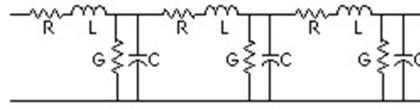
Figure 41. Transmission line structure repeated

The above equations can be solved for an infinite transmission line excited at $x = 0$ by an excitation $V_{in}(t)$ representing the effect of the short on the voltage. The solution for the voltage is:

$$V(x,t) \approx V_{in}\left(t - \sqrt{LC}x\right) \cdot$$
$$\exp\left(-\frac{\sqrt{LC}}{2}\left(\frac{R}{L} + \frac{G}{C}\right)x\right) \tag{33}$$

The above solution describes a voltage signal propagating at a velocity:

$$v = \frac{1}{\sqrt{LC}} \tag{34}$$

and an exponential decay with a decay factor of:

$$\alpha = \frac{\sqrt{LC}}{2}\left(\frac{R}{L} + \frac{G}{C}\right). \tag{35}$$

Assuming the transmission line to be a two-wire cable as described earlier, the following parameters are obtained [26]:

$$R = \frac{2R_S}{\pi d}, \qquad L = \frac{\mu}{\pi \cosh^{-1}\left(\frac{D}{d}\right)},$$
$$G = \frac{\pi\sigma}{\cosh^{-1}\left(\frac{D}{d}\right)}, \qquad C = \frac{\pi\varepsilon}{\cosh^{-1}\left(\frac{D}{d}\right)} \tag{36}$$

where each wire has a diameter d, and the distance between the wires is D. The material between the wires has a permittivity ε, permeability μ and (a very small) conductivity σ. The wire resistance is calculated, as in equation (20), using the surface resistance given in equation (19). The short propagation velocity (34) can be now calculated using the parameters of equation (36), to yield:

$$v = \frac{1}{\sqrt{\varepsilon\mu}} = \frac{c}{n} \tag{37}$$

where, n is the index of refraction around the transmission line. It should be noted that the electromagnetic wave is propagating in the region between the conductors and not in the conductors themselves, where the propagation is much slower and the decay is very strong. We notice the if the two wires are surrounded by air $n \simeq 1$ we recover the velocity of equation (13).

Notice that since according to equation (20) and equation (19) the resistance is frequency dependent as dictated by the skin effect, the resistance term in equation (32) is not a simple multiplication and should be replaced by a convolution. Thus a frequency domain formalism is more adequate to this type of problem as will be described next.

4.2. The frequency domain

In the frequency domain, the telegraph equation takes the form [26]:

$$\begin{aligned}
\frac{\partial V(x,\omega)}{\partial x} &= -(R + i\omega L)I(x,\omega) \\
\frac{\partial I(x,\omega)}{\partial x} &= -(G + i\omega C)V(x,\omega), \qquad i \equiv \sqrt{-1}
\end{aligned} \tag{38}$$

Combining these two equations we can separate the voltage and current variables, in terms of the following two equations:

$$\begin{aligned}
\frac{\partial^2 V(x,\omega)}{\partial x^2} &= \gamma^2 V(x,\omega) \\
\frac{\partial^2 I(x,\omega)}{\partial x^2} &= \gamma^2 I(x,\omega)
\end{aligned} \tag{39}$$

where we defined:

$$\gamma \equiv \sqrt{(R + i\omega L)(G + i\omega C)} \tag{40}$$

These equations have a solution of the form:

$$\begin{aligned}
V(x,\omega) &= V^{(+)}(\omega)e^{-\gamma x} + V^{(-)}(\omega)e^{\gamma x} \\
I(x,\omega) &= \frac{1}{Z_0}\left(V^{(+)}(\omega)e^{-\gamma x} - V^{(-)}(\omega)e^{\gamma x}\right)
\end{aligned} \tag{41}$$

The functions $V^{(\pm)}(\omega)$ are derived from the initial conditions. The impedance Z_0 is defined as follows:

$$Z_0 \equiv \sqrt{\frac{R + i\omega L}{G + i\omega C}} \tag{42}$$

In the case where the resistivity and the leakage admittance are small enough, such that:

$$R << \omega L, \qquad G << \omega C \tag{43}$$

we can approximate the impedance:

$$Z_0 \approx \sqrt{\frac{L}{C}} \tag{44}$$

and, the real and imaginary parts of γ take the form:

$$\mathrm{Re}(\gamma) \approx \frac{\sqrt{LC}}{2}\left(\frac{R}{L} + \frac{G}{C}\right) = \alpha, \ \mathrm{Im}(\gamma) \approx \omega\sqrt{LC} \tag{45}$$

As the frequency rises, the approximation becomes more accurate. Hence for the higher frequency fourier components associated with the short formation this approximation is more effective. Notice that while $\mathrm{Re}(\gamma)$ describes absorption and coincides with the same expression for absorption obtained in equation (33), $\mathrm{Im}(\gamma)$ describes propagation.

4.3. Time dependent vs. stationary shorts

Steady state shorts are easily analyzed in transmission line theory, here we shall try to elucidate the connection between the transient phenomena of the short appearance and its asymptotic behaviour as a steady state phenomena. Our model is depicted in figure 42. We assume that the short appears at some point (x=0) in the transmission line, in which continuity of voltage and current dictate:

$$\begin{aligned}
V_1(0,\omega) &= V_2(0,\omega), \\
I_1(0,\omega) &= I_2(0,\omega) + I_{short}(\omega).
\end{aligned} \tag{46}$$
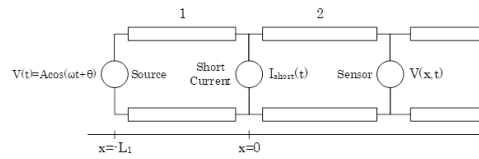
Figure 42. Detailed short in the transmission line model

We assume that the short current doesn't exist at $t = 0$; likewise, the short current after a long time can be calculated using the fact that the voltage on the short vanishes at $t \rightarrow \infty$. The second assumption can be formulated as:

$$\lim_{t \rightarrow \infty} I_{short}(t) = I_{short\ asymptotic}(t) \tag{47}$$

To obtain the asymptotic short current the following calculation is done. First we use the fact that after a considerable duration the voltage on the short vanishes to obtain the following:

$$V_{short\ asymptotic}(\omega) = V^{(+)}(\omega) + V^{(-)}(\omega) = 0 \tag{48}$$

This leads to the result:

$$V^{(-)}(\omega) = -V^{(+)}(\omega) \tag{49}$$

Inserting this result into equation (41) and taking into account that $V_{asymptotic}(\omega, -L_1)$ is the source voltage leads to the following result:

$$
\begin{aligned}
V_{in}(\omega) &= V_{asymptotic}(\omega, -L_1) \\
&= V^{(+)}(\omega)\left(e^{\gamma L_1} - e^{-\gamma L_1}\right)
\end{aligned} \tag{50}
$$

Hence:

$$V^{(+)}(\omega) = \frac{V_{in}(\omega)}{2\sinh(\gamma L_1)} \tag{51}$$

The asymptotic short current in the frequency domain can be calculated using equation (41) at $x = 0$ and taking into account equation (49) and equation (51):

$$
\begin{aligned}
I_{short\ asymptotic}(\omega) &= I(\omega, 0) = \frac{2V^{(+)}}{Z_0} \\
&= \frac{V_{in}(\omega)}{Z_0 \sinh(\gamma L_1)}
\end{aligned} \tag{52}
$$

Taking into account $V_{in}(t)$ given in equation (22) (which is equivalent to a sum of delta functions in the frequency domain) the asymptotic short current in time domain is:

$$I_{short\ asymptotic}(t) = \frac{A_0}{Z_0} \text{Re} \frac{e^{j\omega_0 t}}{\sinh(\gamma(\omega_0)L_1)} \tag{53}$$

The second assumption was that the short current vanishes at $t = 0$:

$$I_{short}(t = 0) = 0 \tag{54}$$

In the current model, this requirement is fulfilled by multiplying the asymptotic expression with some reasonable function that vanishes at $t \rightarrow 0$, and approached unity at $t \rightarrow \infty$ for example:

$$I_{short}(t) = I_{short\ asymptotic}(t) u(t) \left(1 - e^{-\frac{t}{\Delta}}\right) \tag{55}$$

In which $u(t)$ is a step function. The calculation results for the short current on the load side are as follows:

$$
\begin{aligned}
I_2(x,t) \quad = \quad & \frac{e^{-\alpha(x+L_1)}}{Z_0} V_{in}(t - t_{d1}) \\
& - \frac{e^{-\alpha x}}{2} I_{short}(t - t_d) \\
& - \frac{e^{-\alpha(x+2L_1)}}{2} I_{short}(t - t_{d2})
\end{aligned}
\tag{56}
$$

Where $t_d = \frac{x}{v}$, $t_{d1} = \frac{x+L_1}{v}$ and $t_{d2} = \frac{x+2L_1}{v}$. v is a signal propagation velocity. The current in the load side is affected by three terms each with unique retardation. The source voltage is retarded by a time t_{d1} while the short current is retarded by a time t_d for the direct signal and by t_{d2} for the same signal reflected by the circuit source. Each retardation time is proportion to the distance it needs to travel from its source and inversely proportional to velocity of propagation. The model also show that the signals suffer attenuation proportional to the distance they travel.

4.4. Signal dispersion

We now consider the problem of dispersion. This problem is interesting since we would like to know in what ways does the line distort signals propagating on it and in particular how the signal produced by the short is effected. We will start from the definition of γ given in equation (40) and we will assume that $G = 0$. Consequently, the propagation index is:

$$
\gamma(\omega) = i\omega\sqrt{LC}\sqrt{1 + \frac{R}{i\omega L}},
\tag{57}
$$

Now let us investigate the condition:

$$
Ra \equiv \frac{R(\omega)}{i\omega L} \ll 1
\tag{58}
$$

The resistance $R(\omega)$ is frequency dependent due to the skin effect and can be calculated from the surface resistance using equation (19) and equation (20) as follows:

$$
R = \frac{2}{\sqrt{\pi}d}\sqrt{\frac{\mu_c}{\sigma_c}f}
\tag{59}
$$

And thus we obtain the ratio:

$$
\frac{R}{\omega L} = \frac{1}{\sqrt{\pi^3}dL}\sqrt{\frac{\mu_c}{\sigma_c}}\frac{1}{\sqrt{f}}
\tag{60}
$$

Thus the approximation given in equation (58) is even better for higher frequency components. Introducing the inductance impedance:

$$
Z_L = i\omega L = i2\pi f L
\tag{61}
$$

we can cast equation (60) in the form:

$$
\frac{R}{Z_L} \cong -\frac{2.72i}{\sqrt{f}}
\tag{62}
$$

in which the numerical values for the parameters are taken from tables 1, 2 and 5. Equation (62) is depicted in figures 43 which shows that the condition given in equation (58) holds even better for high frequency.
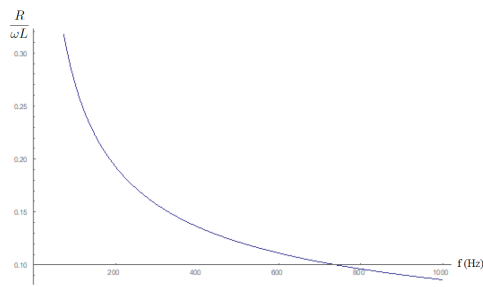
Figure 43. The ratio of resistance to inductance impedance as function of frequency according to equation (62).
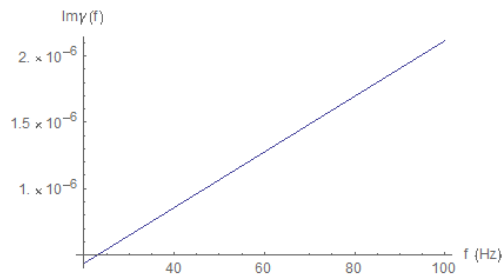
Figure 44. Imγ low frequency dependence

For a small parameter $|x| \ll 1$ we can write:

$$\sqrt{1+x} = 1 + \frac{x}{2} - \frac{x^2}{8} + \frac{x^3}{16} + O[x]^4. \tag{63}$$

Hence taking into account that $\frac{R}{\omega L} \ll 1$, $\gamma(\omega)$ of equation (57) has up to third order the form:

$$\gamma(\omega) \cong j\frac{\omega}{v}\left[1 - j\frac{R}{2\omega L} + \frac{1}{8}\left(\frac{R}{\omega L}\right)^2 + \frac{j}{16}\left(\frac{R}{\omega L}\right)^3\right] \tag{64}$$

This expression can be separated into an imaginary and real parts as follows. The imaginary part of γ takes the form:

$$\mathrm{Im}\gamma \cong \frac{\omega}{v} + \frac{\mu_c}{4\pi^2 d^2 L^2 \sigma_c v} \tag{65}$$

where we have taken in account equation (60). As equation (65) is linear in ω we conclude that there is no dispersion during the signal propagation which requires non linear phase terms. To appreciate the linearity of Imγ we depict it as function of the frequency in both figure 44 for low frequencies and in figure 45 for high frequencies without making an expansion approximation, the linearity and hence the lack of dispersion are apparent for a wide frequency range. For the real part of γ we obtain:
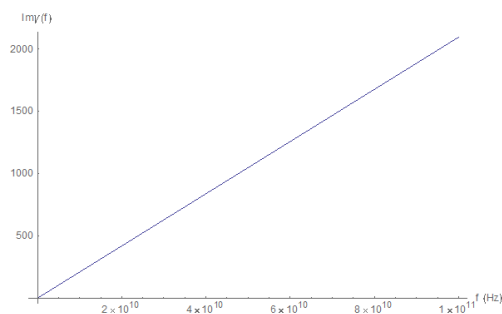
Figure 45. Imγ high frequency dependence
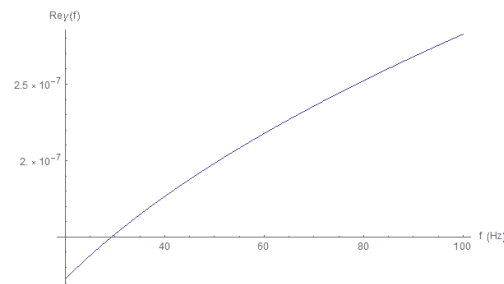
Figure 46. Reγ for low frequencies
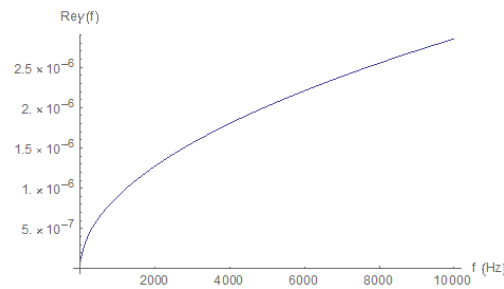
Figure 47. Reγ for high frequencies

$$\mathrm{Re}\gamma \cong \frac{\sqrt{\mu_c}}{2^{\frac{3}{2}}L\sqrt{\sigma_c}\mathrm{v}}\sqrt{\omega} \tag{66}$$

The real part depends on the frequency, but this part is relatively small, compared to the imaginary part. To appreciate the frequency dependence of Reγ we have depicted its behaviour for low frequencies (figure 46), high frequencies (figure 47) and extremely high frequencies (figure 48). To appreciate how small is Reγ with respect to Imγ we plot the ratio of those quantities in figure 49. Another indication to the dominance of Imγ over Reγ is the frequency dependence of $|\gamma|$ which follows quite closely the linear behaviour of Imγ as depicted in figure 50. Finally we remind ourselves that we assumed zero admittance $G = 0$ in our calculations. Practically this means that we have neglected the air admittance with respect to the capacitive admittance:

$$Y_C = i\omega C = i2\pi f C. \tag{67}$$

To check if this assumption is justified we calculate the ratio of the air admittance to capacitive admittance:

$$\frac{G}{Y_C} \simeq -\frac{1.38\ 10^{-6}i}{f} \tag{68}$$

where we have used the parameters of table 3 for the air admittance, and equation (36) for the capacitance. The ratio which is quite small become even smaller for higher frequencies
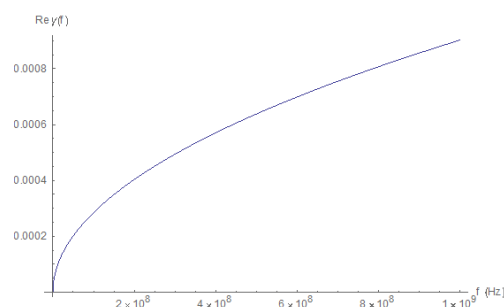
Figure 48. Reγ for very high frequencies
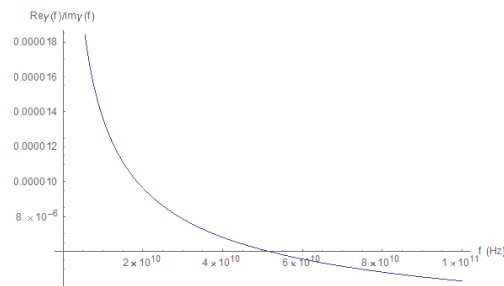
Figure 49. The ratio of real part to imaginary part of γ.
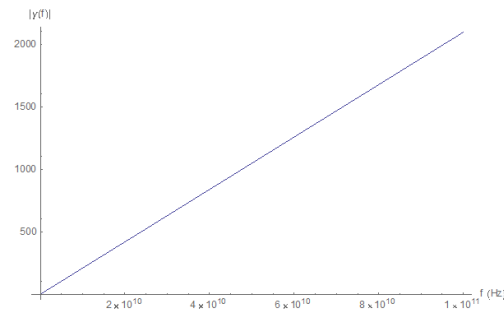
Figure 50. $|\gamma|$ as function of frequency

as depicted in figure 51 and thus justifies our initial assumption. The conclusion of this subsection is that dispersion is not significant in the media in which the pulse generate by the short propagates. This will be further elaborated in the next subsection as we study the prorogation of a signal along the line.

4.5. Signal propagation

We assume that at the entrance to a transmission line we are injecting a short signal of the form:

$$V(0,t) = 2e^{-\frac{t^2}{2\sigma_0^2}}\cos(\omega_0 t) \tag{69}$$

Thus we assume that the short generates a pulse signal while the standard voltage is a periodic trigonometric function of frequency ω_0, which is modulated by the pulse. The pulse is assumed to be Gaussian with a width σ_0. The same signal in the frequency domain will take the form:

$$V(0,\omega) = \sqrt{2\pi}\sigma_0\left(e^{-\frac{\sigma_0^2}{2}(\omega+\omega_0)^2} + e^{-\frac{\sigma_0^2}{2}(\omega-\omega_0)^2}\right) \tag{70}$$

this signal is depicted in figure 52. Now since that signal is injected at the entrance it can propagate in only one direction, hence equation (41) will take the form:

$$V(x,\omega) = V(0,\omega)e^{-\gamma(\omega)x} \tag{71}$$
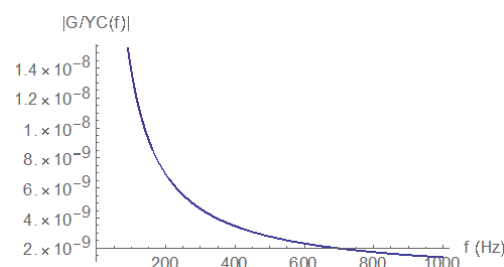
Figure 51. The frequency dependence of $\left|\frac{G}{Y_C}\right|$.
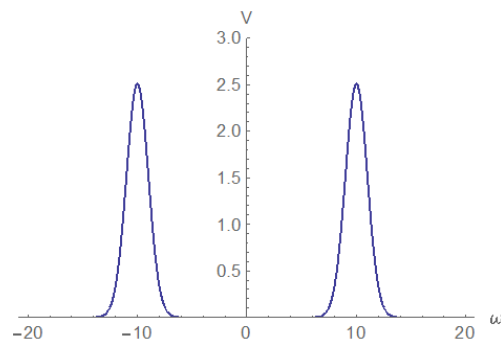
Figure 52. The entrance voltage signal in the frequency domain.

We now expand γ around ω_0 till the second order. This will result in:

$$\gamma(\omega_0 + \omega') \cong \gamma(\omega_0) + \gamma'(\omega_0)\omega' + \frac{1}{2}\gamma''(\omega_0)\omega'^2. \tag{72}$$

Taking into account equation (70), equation (71) and equation (72) and perform an inverse Fourier transform we arrive at the following expression for a propagating signal:

$$V(x,t) = 2\sigma_0 \mathrm{Re}\left[\frac{e^{i\omega_0 t - \gamma_0 x}e^{-\frac{(t-t_d)^2}{2\sigma^2(x)}}}{\sigma(x)}\right] \tag{73}$$

Where the delay time t_d is:

$$t_d = -i\gamma'_0 x = \frac{x}{v}\frac{1 + \frac{3}{4}Ra}{\sqrt{1+Ra}} \cong \frac{x}{v}, \tag{74}$$

hence this is approximately the distance divided by the velocity as expected. We notice that the expression:

$$v_g = |Im\gamma'_0|^{-1} = v\left(\frac{\sqrt{1+Ra}}{1 + \frac{3}{4}Ra}\right), \tag{75}$$

is the group velocity that is the velocity of a wave packet. The width of the signal is:

$$\sigma(x) = \sqrt{\sigma_0{}^2 + \gamma''_0 x} \tag{76}$$

Where:

$$\gamma''_0 = \frac{-iRa\left(1 + \frac{3}{2}Ra\right)}{16v\omega_0\sqrt{1+Ra}^3} \cong -\frac{R(\omega_0)}{16v\omega_0^2 L} \tag{77}$$

The term $\gamma''_0 x$ signifies the pulse broadening as it propagates along the line. Let us assume that $\sigma_0 \approx 10^{-6}$ seconds. For a frequency of 1 MHz and distance of one kilometer:

$$\gamma''_0 x \cong -6.39 \times 10^{-19} - 2.85 \times 10^{-33}i \ll \sigma_0^2 = 10^{-12} \tag{78}$$

hence the dispersion is negligible . However, for a frequency of 1 kHz and a distance of 10 kilometers:

$$\gamma''_0 x \cong -6.39 \times 10^{-12} - 2.85 \times 10^{-17}i \approx \sigma_0^2 = 10^{-12} \tag{79}$$

the widening is comparable to the initial width. Hence despite the fact that dispersion seems small it accumulates over long distances.

4.6. Bifurcations

A power transmission line often bifurcates as depicted in figure 53. In the bifurcation
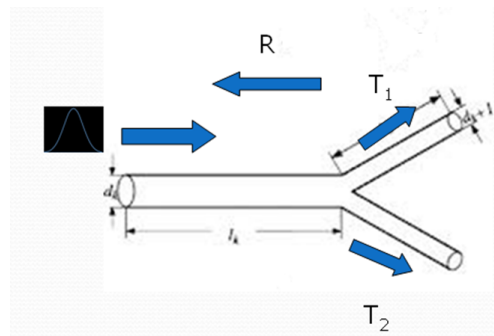
Figure 53. Schematic bifurcation in a power line
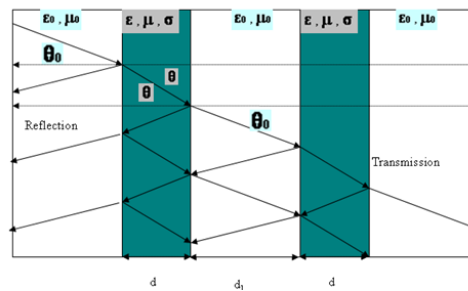
Figure 54. Multiple reflections from a changing propagation media.

junction the signal is transmitted to the bifurcating channels and is also reflected to the original channel in which the short was originally formed. The amount of signal reflected or transmitted is quantified by the reflection R and transmission T coefficients. Those coefficients can in turn be calculated as follows:

$$T_{1\to2} = \frac{2Z_2}{Z_1 + Z_2}, \qquad T_{2\to1} = \frac{2Z_1}{Z_1 + Z_2} \tag{80}$$

$$R_{2\to1} = \frac{Z_2 - Z_1}{Z_1 + Z_2} = -R_{1\to2} \tag{81}$$

in which Z_1 is the impedance of the line before the bifurcation junction and Z_2 is the impedance of the line after the bifurcation junction. In case that the signal meets multiple bifurcation junctions along its path, multiple reflection occur as depicted schematically in figure 54. Multiple reflections will result in multiple signal arriving a the detector as depicted schematically in figure 55. We note that reflected signals arrive at the detector later and in reduced amplitude due to the longer path they need to travel and the additional attenuation the signal suffers during propagation (see equation (73)) and reflection. We note that if a line bifurcates into multiple identical lines as in figure 56, the total impedance
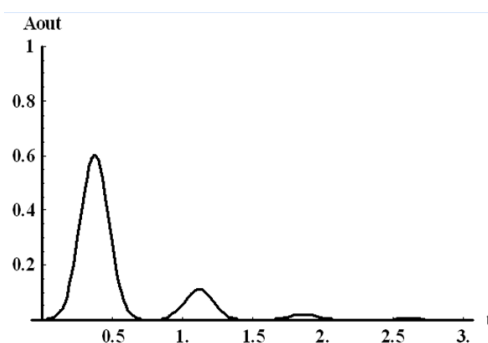
Figure 55. Multiple reflections arriving at the detector.
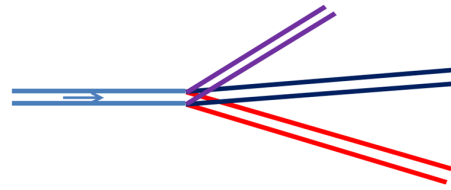
Figure 56. A transmission line bifurcating into multiple channels.
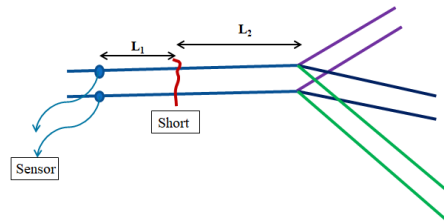
Figure 57. A short occurs between the sensor and the bifurcation point.

at the channel after the bifurcation will be equal to the original impedance Z_0 divided by the number of transmission line N, hence:

$$Z_1 = Z_0, \qquad Z_2 = \frac{Z_0}{N} \tag{82}$$

Which implies according to equation (80) a transmission coefficient of:

$$T_{1 \to 2} = \frac{2Z_2}{Z_1 + Z_2} = \frac{2\frac{Z_0}{N}}{Z_0 + \frac{Z_0}{N}} = \frac{2}{N+1} \tag{83}$$

$$R_{1 \to 2} = \frac{Z_1 - Z_2}{Z_1 + Z_2} = \frac{Z_0 - \frac{Z_0}{N}}{Z_0 + \frac{Z_0}{N}} = \frac{N-1}{N+1} \tag{84}$$

hence for a bifurcation to a large number of channels the reflection coefficient will tend to one, while for a continuation into a single identical channel there will not be obviously a reflection.

We will now examine the reflection effect and see if one can use the reflected signal instead of a second sensor thus reducing the amount of hardware needed in order to implement the method described. First let us look at figure 57, the short occurs between the sensor and the bifurcation point. Thus a signal is propagating from the short to the sensor and an additional signal propagates to the bifurcation point where it is reflected. Provided that the short will not introduce an impenetrable obstacle the signal will eventually reach the detector at a later time. The direct signal arrival time will satisfy according to equation (1):

$$t_1 - t_0 = \frac{L_1}{v} \tag{85}$$

The reflected signal will arrive at a later time such that:

$$t_2 - t_0 = \frac{L_1 + 2L_2}{v} \tag{86}$$

Hence the time difference between the direct and reflected signal allows us to calculate the distance between the short and bifurcation point as:

$$L_2 = \frac{1}{2}v(t_2 - t_1) \tag{87}$$
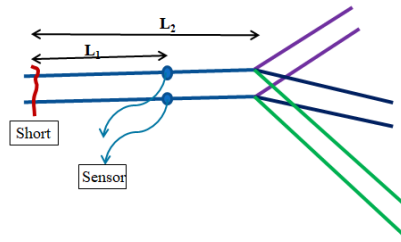
Figure 58. The sensor is between the short and the bifurcation point.
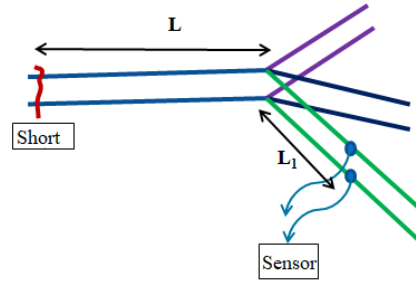
Figure 59. The sensor is on a bifurcation of the transmission line.

now since the distance L between the sensor and bifurcation point is known in advance, we may calculate the distance between the short and the bifurcation point as follows:

$$L_1 = L - L_2 = L - \frac{1}{2}v(t_2 - t_1) \tag{88}$$

Thus in this case a single detector will suffice and we will not need two detectors as described in section 2. This will reduce the cost of the system and will make redundant issues like sensor synchronization. A last advantageous scenario is depicted in figure 58 The direct signal arrival time will satisfy according to equation (1):

$$t_1 - t_0 = \frac{L_1}{v} \tag{89}$$

The reflected signal will arrive at a later time such that:

$$t_2 - t_0 = \frac{2L_2 - L_1}{v} \tag{90}$$

The time difference in this case will yield:

$$L_2 - L_1 = \frac{1}{2}v(t_2 - t_1) \tag{91}$$

which does not reveal any information on the short location but rather some trivial information on the distance between the sensor and the bifurcation point which is already known. Of course if there exist additional bifurcation points on the signal path (for example left to the short) then we are at the previous case again and one sensor will suffice. We may deduce that putting sensors on bifurcation points will reduce the amount of sensors needed. Finally we look at the case in which the signal arrives to a sensor located after the branching point of the net as in figure 59. The sensor will receive a signal at:

$$t_1 - t_0 = \frac{L + L_1}{v} \tag{92}$$
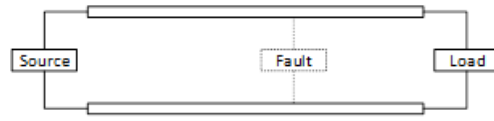
Figure 60. Schematics of the fault scenario
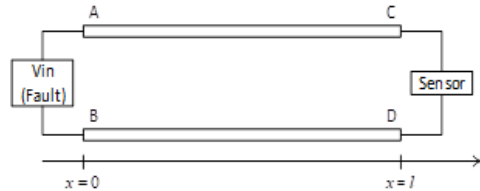
Figure 61. Schematics of the fault modeling

this will not suffice to locate the short unless a reflected signal will be received from another point along the network. To conclude, we deduce that putting sensors on bifurcation points will reduce the amount of sensors needed along the network. Moreover, relying on reflections may solve the problem of sensor synchronization.

4.7. Laplace analysis

We will now address the transmission line pulse propagation problem using the technique of Laplace analysis [27]. The simplified power system of our interest may be schematically presented in figure 60 . The fault produces two separate signals propagating towards the source and the load, where sensors are located. In each section, as a result of the fault, the voltage perturbation is perceived as an input signal, propagating towards a sensor, as shown in Figure 61. In the transmission line, we assume the validity of the telegraph equations (38) and replace $i\omega \rightarrow s$. The Laplace form of the telegraph equations admits the solution:

$$V(x,s) = V_{(-)}(s)e^{-x\gamma(s)} + V_{(+)}(s)e^{x\gamma(s)} \tag{93}$$

$$I(x,s) = \frac{V_{(-)}(s)}{Z_0(s)}e^{-x\gamma(s)} - \frac{V_{(+)}(s)}{Z_0(s)}e^{x\gamma(s)} \tag{94}$$

where,

$$Z(s) = R + sL, \ Y(s) = G + sC \tag{95}$$

$$\gamma(s) = \sqrt{Z(s)Y(s)} \tag{96}$$

$$Z_0(s) = \sqrt{\frac{Z(s)}{Y(s)}} \tag{97}$$

It is realistic to presume that the conductance G of the separating dielectric material between the wires, is insignificant. The series resistivity is calculated taking into account the skin effect:

$$R(s) = \frac{1}{\pi d}\sqrt{\frac{2\mu_c}{\sigma_c}}\sqrt{s} \equiv \xi\sqrt{s} \tag{98}$$

where d is a conductor wire diameter and:

$$\xi = \frac{1}{\pi d}\sqrt{\frac{2\mu_c}{\sigma_c}}. \tag{99}$$

Consequently, the expression (96) can be written as follows:

$$
\begin{aligned}
\gamma(s) = s\sqrt{LC}\sqrt{1 + \frac{R(s)}{sL}} = s\sqrt{LC}\sqrt{1 + \frac{\xi}{\sqrt{s}L}} \approx \\
\approx s\sqrt{LC}\left(1 + \frac{\xi}{2\sqrt{s}L}\right) = s\sqrt{LC} + \frac{\xi}{2}\sqrt{\frac{C}{L}}\sqrt{s}
\end{aligned}
\tag{100}
$$

The sensor impedance Z_L is designed to be infinite so as not to influence the measurement results. Substituting boundary conditions,

$$
V_{fault}(s) = V(0,s) = V_{(-)}(s) + V_{(+)}(s)
\tag{101}
$$

and:

$$
Z_L = \infty
\tag{102}
$$

which implies zero current at $x = l$:

$$
I(l,s) = \frac{V_{(-)}(s)}{Z_0(s)}e^{-l\gamma(s)} - \frac{V_{(+)}(s)}{Z_0(s)}e^{l\gamma(s)} = 0
\tag{103}
$$

or:

$$
V_{(-)}(s) = V_{(+)}(s)e^{2l\gamma(s)}
\tag{104}
$$

Combining the above equation with equation (101) yields:

$$
V_{(+)} = \frac{V_{fault}(s)}{1 + e^{2l\gamma(s)}}
\tag{105}
$$

and

$$
V_{(-)} = \frac{V_{fault}(s)}{1 + e^{-2l\gamma(s)}}
\tag{106}
$$

The voltage signal at the sensor due to the fault is thus:

$$
V_{out}(s) \equiv V(l,s) = \frac{2e^{-l\gamma(s)}}{1 + e^{-2l\gamma(s)}}V_{fault}(s)
\tag{107}
$$

Identifying the last expression as the summation of a geometric series, it can be re-written as the sum:

$$
V_{out}(s) = 2V_{fault}(s)\sum_{n=0}^{\infty}(-1)^n e^{-(1+2n)l\gamma(s)}
\tag{108}
$$

Defining:

$$
\tau_n \equiv (1+2n)l\sqrt{LC}
\tag{109}
$$

and

$$
B_n \equiv (1+2n)l\frac{\xi}{2}\sqrt{\frac{C}{L}}
\tag{110}
$$

the expression for the voltage at the sensor equation (108) takes the form:

$$
V_{out}(s) = 2V_{fault}(s)\sum_{n=0}^{\infty}(-1)^n e^{-\tau_n s + B_n\sqrt{s}}
\tag{111}
$$

This sum can be interpreted as the sum of multiple reflected waves each with its unique delay time. The system's transfer function may be now calculated as follows:

$$
H(s) \equiv \frac{V_{out}(s)}{V_{fault}(s)} = 2\sum_{n=0}^{\infty}(-1)^n e^{-\tau_n s + B_n\sqrt{s}}
\tag{112}
$$
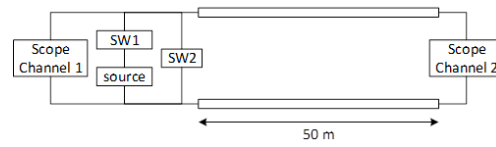
Figure 62. Schematics of the experimental setup

this allows for obtaining the signal measured at the sensor, due to any fault waveform. For example, if the fault is a sudden short circuit at $x = 0$ and $t = 0$, the voltage at the fault location is:

$$V_{in}(t) \equiv V(0, t) = V_0 - V_0 u(t). \tag{113}$$

Using the superposition principle, $V_{out}(t)$ may be expressed as the sum of a DC input and a step function input response.

$$V_{out}(t) = V_{out(V_{in}=V_0)}(t) - V_{out(V_{in}=V_0 u(t))}(t) \tag{114}$$

Since the impedance at the edge is infinite, the voltage along the line due to the DC input is simply V_0. Moreover, the Laplace transform of a step function satisfies:

$$\mathcal{L}\{u(t)\} = \frac{1}{s}, \tag{115}$$

hence:

$$V_{out(V_{in}=V_0 u(t))}(s) = \frac{V_0 H(s)}{s} \tag{116}$$

Hence using the transfer function definition equation (112), and performing an inverse transform back to the time domain, we obtain:

$$V_{out}(t) = V_0 - 2\mathcal{L}^{-1}\left\{ \frac{V_0}{s} \sum_{n=0}^{\infty} (-1)^n e^{-\tau_n s + B_n \sqrt{s}} \right\} \tag{117}$$

Taking a known inverse Laplace transform [19]:

$$\mathcal{L}^{-1}\left\{ e^{-\tau s} \frac{e^{-B\sqrt{s}}}{s} \right\} = erfc\left(\frac{B}{2\sqrt{t - \tau}} \right) u(t - \tau) \tag{118}$$

The voltage at the sensor, as a result of fault, is:

$$V_{out}(t) = V_0 - 2V_0 \sum_{n=0}^{\infty} (-1)^n erfc\left(\frac{B_n}{2\sqrt{t - \tau_n}} \right)$$
$$u(t - \tau_n) \tag{119}$$

The above result will suffice if the rise time of the short is fast enough and could be ignored.

5. Experimental setup
5.1. Experiment hardware

An experimental demonstration of the fault location technique involves the setup shown schematically in figure 62, in which 10V DC voltage is supplied from a TTi QL355TP power supply source, shown in Figure 63 to 50m two-wire cable and switches. The sensor is a MS09404A Mixed Signal Oscilloscope of 4 GHz bandwidth, which has two channels, as shown in figure 64. Figure 65 illustrates the dimensions of the transmission line. The transmission line is comprised of a two-wire power cord. Each wire is made of copper and is $d = 1$ mm in diameter, the distance between the wires is $D = 4$ mm. These parameters

Figure 63. TTi QL355TP power supply

Figure 64. MS09404A Mixed Signal Oscilloscope of 4 GHz bandwidth having two channels
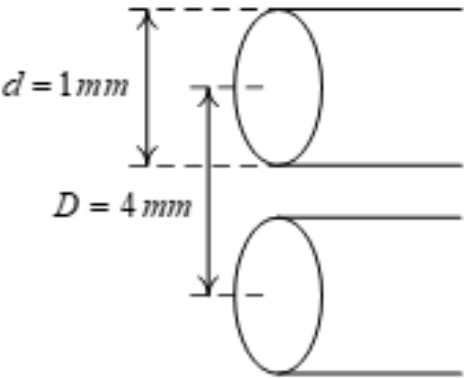
Figure 65. Dimensions of the transmission line
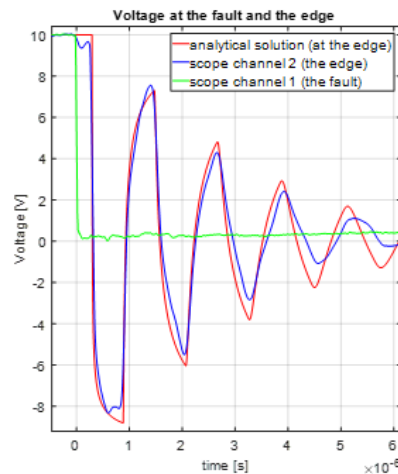
Figure 66. Comparison of experimental results and theoretical predictions of equation (119) for the measured voltage.

allow us to calculate the inductance L and capacitance C, from the dielectric constant, magnetic permeability and conductivity as follows (see equation (36)):

$$\varepsilon_{r(insulator)} = 3.45, \mu_{r(insulator)} = 1,$$

$$\sigma_{copper} = 3 \ 10^6 \frac{S}{m}, n = \sqrt{\varepsilon_r \mu_r} \simeq 1.86$$

$$C = \frac{2\pi\varepsilon}{\cosh^{-1}\left(\frac{D^2 - 2d^2}{2d^2}\right)} = 7.22 \ 10^{-11} \frac{F}{m}$$

$$L = \frac{\varepsilon\mu}{C} = 5.27 \ 10^{-7} \frac{H}{m} \tag{120}$$

5.2. Experimental process

On one side of the transmission line, we connected the DC source, 2 switches and the scope channel; another channel is connected to the other side. Closing the first switch when the second switch is open, we obtain a steady state DC voltage along the line. The short circuit fault is achieved by closing the second switch.

6. Results and data processing

6.1. Location accuracy

Measuring the voltage of both sides of the line, we can see clearly the delay in signal propagation along the line. Additional reflected waves (figures 66 and 67) are also seen. The scope channel data is exported and processed using the MATLAB software. Our aim is of course to discover how long it takes the signal to arrive from the fault to the measuring point. Because the waves arriving at the edge are reflected in the opposite direction (towards the fault), where they are repeatedly reflected, one fault may supply several data points that we can process to our advantage, depending on how fast the transient signals decay. In this study, it was possible to measure five signals (peaks) each time, and so choose the optimal data processing technique.

To obtain the best accuracy, we performed numerous Voltage smoothing and Voltage derivative smoothing changing the time window and thus the number of samples. Obviously the wider the window the less noise we have to distort our results. However, a wide window may distort the reflection signal as well, compromising our accuracy. We used five different averaging windows and thus obtained five different errors for each reflection. The data is given in the appendix, in the table each line represent a different values of Voltage
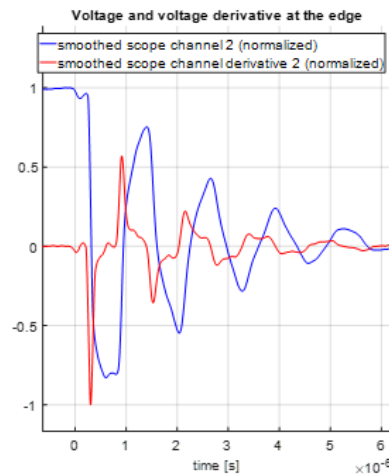
Figure 67. Comparison of sensor voltage and its derivative.
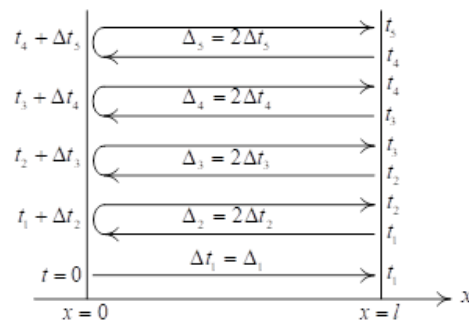
Figure 68. The propagation times for the pulse reflections.

smoothing window and Voltage derivative smoothing window and errors which have been deduced for each reflection and processing method.

Figure 67 shows that the voltage derivative peaks are much sharper; therefore, the short circuit fault location is calculated by finding the time intervals between the local extremum points in the voltage derivative at the transmission line edge. In addition, the smoothing filter window may slightly change the results, and the optimum configuration was 200 points in a window. In this situation, the accuracy in the short circuit fault location detection is $\pm 0.005\%$ using the second peak.

This can be compared to the theoretical accuracy predicted by equation (11). In the current case the sampling rate is $4\,\text{GHz}$ and hence the time between samples is $T = 2.5\,10^{-10}$ seconds and the velocity is $v = \frac{c}{n} = 1.62\,10^{8}$ meters/second. Thus the accuracy may be as high as 0.008 meters which is $\pm 0.008\%$ quite close to the best experimental result. This indicates that the theoretical limit is achievable provided the data is processed correctly.

6.2. Comparison with theory

We now compare the results of the theory given in equation (119) to the (smoothed) experimental results. The results of the comparison are depicted in figure 69. The signal reflection scheme is shown in figure 68. The unprocessed timings of various peaks are correlated with signal reflections and are given in table 6. The same results derived from a theoretical calculation are given in table 7. Obviously the theoretical distance evaluation is better than the experimental, however, processing dramatically improves the situation as we saw in the previous section. The distances can be derived from the time differences as follows:

$$\Delta L = v\,\Delta t = \frac{c\Delta t}{\sqrt{\varepsilon_r \mu_r}} = \frac{3\,10^8}{\sqrt{3.45}}\Delta t \tag{121}$$

Table 6. Distance calculations based on raw data without applying any processing technique

$t_i[s]$	$\Delta_i[s]$	$\Delta t_i[s]$	ΔL	$error[\%]$
4.5 10^{-7}		4.5 10^{-7}	79	-21%
1.5 10^{-6}	1.0 10^{-6}	5.2 10^{-7}	90	-10%
2.8 10^{-6}	1.3 10^{-6}	6.5 10^{-7}	113	13%
4.1 10^{-6}	1.3 10^{-6}	6.5 10^{-7}	113	13%
5.4 10^{-6}	1.3 10^{-6}	6.6 10^{-7}	114	14%

Table 7. Distance calculations from simulation results.

$t_j[s]$	$\delta_j[s]$	$\Delta t'_I[s]$	L'
5.8 10^{-7}		5.8 10^{-7}	100
1.7 10^{-6}	1.2 10^{-6}	5.8 10^{-7}	101
2.9 10^{-6}	1.2 10^{-6}	5.9 10^{-7}	102
4.2 10^{-6}	1.2 10^{-6}	6.2 10^{-7}	107
5.3 10^{-6}	1.2 10^{-6}	5.9 10^{-7}	102

In the above we denote Δt_i and $\Delta t'_i$ for one direction experimental and theoretical propagation times, respectively. As we can see, the propagation times are sufficiently stable and consistent with the theoretical model. Hence, the pulse location information can also be obtained from the voltage signal (without signal derivative if precision is not required).

However, there is a difference between theoretical and the experimental graphs. In the experimental data, there are additional peaks in the first reflected waves; after the third (main) peak, the "oscillation" frequency is twice as great as in the theoretical model. This is because of the reflected waves from the middle of the transmission line: in the experimental setup, the line is not homogeneous as can be deduced from the additional peaks we receive.

Finally we present the comparison of theoretical and empirical derivatives given in figure 65. The timing of peak derivatives seem to fit much better the theoretical curve and the location errors are much smaller. As noted previously processing may improve the accuracy drastically.

7. SYNCHRONIZATION BETWEEN SENSORS MEASUREMENTS

Before measuring a transient phenomenon [30], an accurate method for measuring it must be chosen [31]. According to a broad literary review of a shelf product that will be used as a final product for synchronization between the measurements of the sensors at the same time, it was found that The White Rabbit is a (PTP - Precision Time Protocol) Application for Robust Sub-Nanosecond Synchronization [32], Characteristics and Research applications in technology, See [33], [34], [35].

Table 8. Distance calculations from signal derivatives and respective location errors

	t_i	Δt_i	ΔL	error [%]
1	3.11 10^{-7}		52.1	4.28%
2	9.16 10^{-7}	6.06 10^{-7}	101.5	1.55%
3	1.52 10^{-6}	6.08 10^{-7}	101.9	1.90%
4	2.16 10^{-6}	6.31 10^{-7}	105.8	5.82%
5	2.77 10^{-6}	6.15 10^{-7}	103.1	3.14%
6	3.40 10^{-6}	6.28 10^{-7}	105.3	5.32%

Table 9. Comparison of fault location accuracy methods. DSE - Distribution State Estimation algorithm. SMT - Synchronised Measurement Technology.

Method	Acc.(%)	Refer.
The developed algorithm	0.005	Here
Algorithm based on date measured at both ends of two terminal single high voltage transmission line	0.01	[27]
H-matrix and the measurements of V and C	3.226	[28]
Varying the fault resistance fault locations algorithm	0.81	[29]
Proposed Algor.	12.58	[1]
Simple Ohm's Law	16.22	[1]
Absol.Value Imped.	16.17	[1]
Loop React.	21.98	[1]
Takagi	17.45	[1]
Santoso et al.'s Algorithm	14.4-17.5	[1]
Impedance-based method	3.91	[2]
(DSE)	large	[3]
Fuzzy inference	5	[4]
HV travel-waves	0.78	[5]
(SMT)	3	[6]

8. Conclusions and Summary

In the framework of the current research, a propagation of a short signal in a two-wire cable was investigated. It was shown that the short can be detected either by voltage or current measurements or by taking the voltage/current first or second derivatives. By measuring the voltage or current derivatives, the short can be detected either on the source or the load side. It was also shown that using bifurcations and reflection the amount of detectors may be reduced. In order to achieve a high level of accuracy regarding the short's location, the inter sampling duration should be of the nanosecond order (sampling frequency of GHz). Of course, if there is no significant slope over a predetermined number of samples (say 1,000 samples), there is no need to save them. Hence, the samples may be written as a moving window to some buffer register and deleted if the gradient is not significant. We have also studied the phenomena of dispersion of the short signal and determined in what situations it is significant.

Our method is based on the idea that in any system information even in the form of an electromagnetic wave will advance from one side of the system to the other in a fast but finite velocity v stratifying $v < c$, c is the speed of light in vacuum.

When considering steady state we may neglect the propagation phenomena and employ lumped models, however, this is not applicable for short durations as considered here.

The accuracy is significantly better in the retardation approach than in various methods mentioned in previous art (neglecting the propagation phenomena). In table 9 the accuracy of the different methods is compared.

It is expected that in the future, better wave sampling techniques and devices will be developed and better processing methodologies thus improving accuracy.

The above system description was derived for an electrical transmission line as the wave behavior is well-known and there is considerable expertise in making the calculations; however, the same holds true for optical fibers and optical reflections as well as for pipes, such as water, gas or oil pipes and acoustic echoes. The calculations for the fault's location are the same, although the propagation rates are different in the acoustic case. In the optical case, the equation $v = \frac{c}{n}$ still holds true. In both cases, underground pipes and underground fiber optic cables can be damaged at hard-to-reach locations, and an accurate determination of the fault's location is helpful in knowing where to start digging.
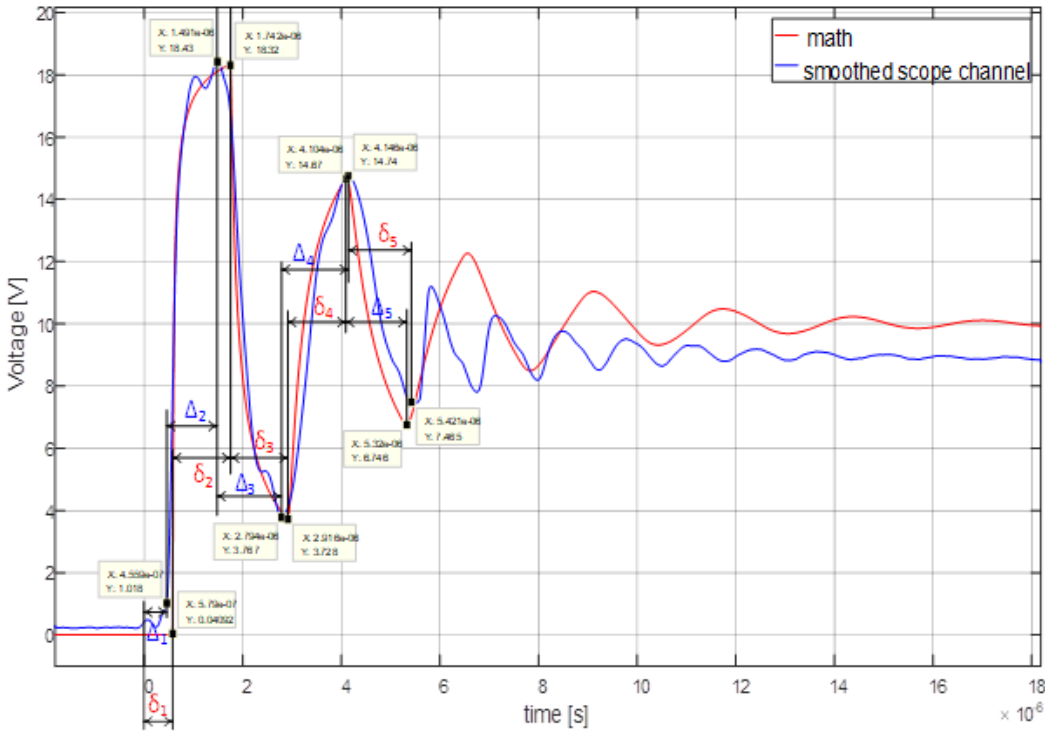
Figure 69. Comparison results between equation (119) and smoothed scope channel.
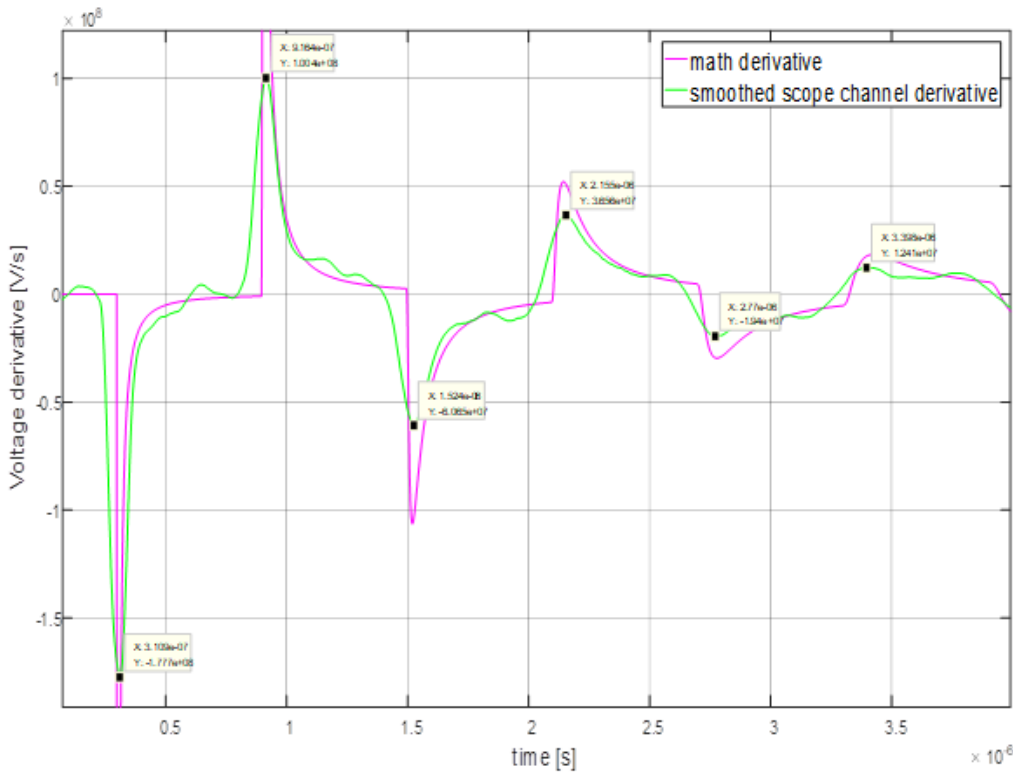

Figure 70. Comparison between theoretical derivative and smoothed scope channel derivative.

1. A. Einstein, "On the Electrodynamics of Moving Bodies", Annalen der Physik 17 (10): 891–921, (1905).
2. Kulkarni, Saurabh Shirish, *"Fault location and characterization in AC and DC power systems"* (2012)
3. Ghimire, Sushma, *"Analysis of Fault location methods on transmission lines"*, (2014)
4. Xu, Zhihan? *"Fault location and incipient fault detection in distribution cables"*, (2011)
5. Chen, Kunjin and Huang, Caowei and He, Jinliang, *Fault detection, classification and location for transmission lines and distribution systems: a review on the methods*, (High voltage,volume 1, number 1, pages 25–33, IET 2016)
6. Glik, Krzysztof and Rasolomampionona, Désiré Dauphin and Kowalik, Ryszard, *"Detection, classification and fault location in HV lines using travelling waves"*, (journal Przeglad Elektrotechniczny (Electrical Review), volume 88, number 1A, pages 269–275, 2012)
7. Radojević, ZM and Kim, CH and Popov, M and Preston, G and Terzija, V, *"New approach for fault location on transmission lines not requiring line parameters"*, International Conference on Power System Transients Proceedings, (2009)
8. M. Patel and R. N. Patel, "2015 2nd International Conference on Signal Processing and Integrated Networks (SPIN)", *"Fault analysis in transmission lines using neural network and wavelets"*, (doi 10.1109/SPIN.2015.7095386, pages 719-724, Feb 2015)
9. Bunnoon, Pituk, *"Fault detection approaches to power system: state-of-the-art article reviews for searching a new approach in the future"*, (International Journal of Electrical and Computer Engineering,volume 3, number 4, pages 553, IAES Institute of Advanced Engineering and Science, 2013)
10. Dong Aihua and Huo Liuhang and Li Liang and Wang Qingxuan, *"2010 International Conference on Computer and Communication Technologies in Agriculture Engineering"*, "Research on the practical detection for a power cable fault point", (doi 10.1109/CCTAE.2010.5544072, volume 2, pages 80-84, ISSN 2161-1092, June 2010)
11. M. N. Alam and R. H. Bhuiyan and R. Dougal and M. Ali, *"2011 IEEE International Symposium on Antennas and Propagation (APSURSI)"*, *"Novel surface wave exciters for power line fault detection and communications"*, (doi 10.1109/APS.2011.5996484, pages 1139-1142, July 2011)
12. M. Aldeen and F. Crusca, *"IEE Proceedings - Generation, Transmission and Distribution"*, *"Observer-based fault detection and identification scheme for power systems"*, (doi 10.1049/ip-gtd:20045101, volume 153, number 1, pages 71-79, ISSN 1350-2360, Jan 2006)
13. Q. Alsafasfeh and I. Abdel-Qader and A. Harb, *"2010 IEEE International Conference on Electro/Information Technology"*, *"Symmetrical pattern and PCA based framework for fault detection and classification in power systems"*, (doi 10.1109/EIT.2010.5612179, pages 1-5, ISSN 2154-0357, May 2010)
14. A. Ashouri and A. Jalilvand and R. Noroozian and A. Bagheri, *"2010 Joint International Conference on Power Electronics, Drives and Energy Systems 2010 Power India"*, *"A new approach for fault detection in digital relays-based power system using Petri nets"*, (doi 10.1109/PEDES.2010.5712527, pages 1-8, Dec 2010)
15. A. Bhoomaiah and P. K. Reddy and K. S. L. Murthy and P. A. Naidu and B. P. Singh, *"The 17th Annual Meeting of the IEEE Lasers and Electro-Optics Society, 2004. LEOS 2004"*, *"Measurement of neutral currents in a power transformer and fault detection using wavelet techniques"*, (doi 10.1109/CEIDP.2004.1364216,pages 170-173, Oct 2004)
16. R. Dubey and S. R. Samantaray and A. Tripathy and B. C. Babu and M. Ehtesham, *"2012 Students Conference on Engineering and Systems"*, *"Wavelet based energy function for symmetrical fault detection during power swing"*, (doi 10.1109/SCES.2012.6199019, pages 1-6, March 2012)
17. H. Shu and Wang Xu and Tian Xincui and Wu Qianjin and S. Peng, *"2010 2nd International Conference on Industrial and Information Systems"*, *"On the use of S-transform for fault feeder detection based on two phase currents in distribution power systems"*, (doi 10.1109/INDUSIS.2010.5565706, volume 2, pages 282-287, July 2010)
18. Zhiling Long and N. H. Younan and T. O. Bialek, *"2012 International Conference on High Voltage Engineering and Application"*, *"Underground power cable fault detection using complex wavelet analysis"*, (doi 10.1109/ICHVE.2012.6357058, pages 59-62, Sept 2012)
19. Magnusson, Philip C and Tripathi, Vijai K and Alexander, Gerald C and Weisshaar, Andreas, *"Transmission lines and wave propagation"*, (CRC Press, 2000)
20. FARAHMAND, DR FARID, *"Introduction to Transmission Lines"*, (A Primer on Electromagnetic Fields; International Publishers Association: Geneva, Switzerland, 2012)
21. Hui, Hon Tat, *"Transmission Lines–Basic Theories"*, (NUS/ECE Lecture Notes, 2011)
22. Matzner, H. and Levy, S., *"Experiment 3 – Transmission Lines, Part 1"*, (August 2008)

23. M. Nabwani, M. Suleymanov, Y. Pinhasi & A. Yahalom "Retardation in the Service of Real Time Fault Detection and the Difference Between Distributed and Lumped Fault Models" Proceedings of the Material Technologies and Modeling the Tenth International Conference, Ariel University, Ariel, Israel, August 20 – 24, 2018.

24. Yosef Pinhasi & Asher Yahalom "Fault Location in a Transmission Line" USA Patent US11079422B2 (claiming priority to US Provisional Application No. 62/309,550, filed March 17, 2016). 03/08/21 application granted.

25. Yosef Pinhasi & Asher Yahalom "Fault Location in a Transmission Line" IL Patent 261763, filed 17/03/2017 (claiming priority to US Provisional Application No. 62/309,550, filed March 17, 2016). Publication date 31/10/2018, allowed 12/07/21, 31/10/21 Publication of IL261763A.

26. David M. Pozar "Microwave Engineering", Fourth Edition. (John Wiley & Sons, 2012)

27. Michael Sulymanov, Asher Yahalom and Yosef Pinhasi "Real Time Fault Location in High Voltage Network Power Lines". Proceedings of the 2016 ICSEE International Conference on the Science of Electrical Engineering, November 16 – 18, 2016, Hilton Queen of Sheba, Eilat, Israel. DOI: 10.1109/ICSEE.2016.7806061

28. ANKAMMA RAO J, BIZUAYEHU BOGALE, JEMAL MOHAMMED AMIN and TSEGAYE NEGASH GIZAW " FAULT LOCATION CALCULATION BASED ON TWO TERMINAL DATA HIGH VOLTAGE TRANMISSION LINE", International Journal of Research in Engineering and Technology (IMPACT: IJRET), ISSN (P): 2347-4599; ISSN (E): 2321-8843, Vol. 4, Issue 10, Oct 2016, 1-8.

29. Josef Tlustý, Jaroslav Doležal, Jan Kyncl, Radek Hanuš " FAULT LOCATION IN HV SYSTEMS", The financial support of the Ministry of Education, Youth and Sports (Research Plan MSM 6840770017 of the Czech Technical University) is highly acknowledged.

30. Jianwei Li, Qingqing Yang, Hao Mu, Simon Le Blond, Hongwen He, " A new fault detection and fault location method for multi-terminal high voltage direct current of offshore wind farm", Applied Energy 220 (2018) 13-20.

31. Arieh Shenkman, "Transient Analysis of Electric Power Circuits Handbook", page 466, 2005, Springer.

32. Guide for Measurement of Radio Frequency Interference From Hv And Mv Substations, Draft 6a, May 2008, CIRED/CIGRÉ JWG C4.202

33. "White Rabbit: a PTP application for robust sub-nanosecond synchronization" M. Lipiński, T. Włostowski, J. Serrano, P. Alvarez, Proceedings of ISPCS2011, Munich, Germany, 2011

34. "Digital Dual Mixer Time Difference for Sub-Nanosecond Time Synchronization in Ethernet" P. Moreira, P. Alvarez, J.Serrano, I. Darwezeh, T. Wlostowski, Frequency Control Symposium (FCS), 2010.

35. "White Rabbit clock characteristics" M. Rizzi, M. Lipinski, T. Wlostowski J. Serrano, S. Ferrari, S. Rinaldi, Proceedings of ISPCS2016, Stockholm, Sweden

36. "Precise time and frequency transfer in a White Rabbit network" T. Wlostowski, Warsaw University of Technology, Warsaw, Poland, 2010

Appendix: Errors received of smoothing Voltage and derivative smoothing Voltage window

Voltage smoothing window	Voltage derivative smoothing window	Error$_1$ [%]	Error$_2$ [%]	Error$_3$ [%]	Error$_4$ [%]	Error$_5$ [%]	max(abs(error))	mean(abs(error))	max(error)-min(error)
50	50	-1.80	-2.06	2.98	1.56	-5.03	5.03	2.69	8.01
50	100	-2.06	-1.93	1.95	1.04	-1.41	2.06	1.68	4.01
50	150	-3.48	-2.32	1.04	0.91	1.56	3.48	1.86	5.04
50	200	-4.12	-3.35	2.34	0.01	-0.89	4.12	2.14	6.46
50	250	-5.16	-2.19	2.46	-0.51	-0.51	5.16	2.16	7.62
50	300	-2.96	-2.45	1.17	2.46	-0.64	2.96	1.94	5.43
50	350	-4.25	-4.64	2.98	2.59	-0.89	4.64	3.07	7.62
50	400	-2.06	-4.51	1.56	2.98	0.53	4.51	2.33	7.49
50	450	-3.22	-3.22	1.43	2.46	1.43	3.22	2.35	5.69
50	500	0.01	-2.83	1.82	3.76	4.66	4.66	2.62	7.49
50	550	5.70	-2.06	0.91	3.89	2.85	5.70	3.08	7.75
50	600	11.51	-2.32	0.66	2.85	3.89	11.51	4.24	13.83
100	50	-2.06	-1.93	1.95	1.04	-1.41	2.06	1.68	4.01
100	100	-1.28	-1.15	1.43	1.43	1.56	1.56	1.37	2.84
100	150	-2.06	-1.02	1.17	1.56	0.01	2.06	1.16	3.62
100	200	-2.83	-2.06	2.08	1.43	-1.02	2.83	1.88	4.91
100	250	-3.74	-2.32	2.21	1.56	-1.28	3.74	2.22	5.94
100	300	-3.87	-2.83	1.69	2.34	0.53	3.87	2.25	6.20
100	350	-3.48	-3.74	1.82	3.63	-0.38	3.74	2.61	7.37
100	400	-3.48	-3.61	1.43	3.50	0.14	3.61	2.43	7.11
100	450	-0.89	-3.48	0.79	3.24	1.69	3.48	2.02	6.72
100	500	0.53	-2.83	0.27	5.18	2.21	5.18	2.20	8.01
100	550	3.89	-2.83	0.66	4.79	1.95	4.79	2.82	7.62
100	600	9.44	-1.28	-0.12	3.50	2.21	9.44	3.31	10.72
150	50	-3.48	-2.32	1.04	0.91	1.56	3.48	1.86	5.04
150	100	-2.06	-1.02	1.17	1.56	0.01	2.06	1.16	3.62
150	150	-0.77	-0.38	2.08	0.79	0.01	2.08	0.80	2.84
150	200	-1.67	-0.64	2.98	1.56	0.14	2.98	1.40	4.65
150	250	-2.70	-1.02	2.59	2.85	-0.89	2.85	2.01	5.56
150	300	-2.83	-1.80	2.85	3.24	0.01	3.24	2.15	6.07
150	350	-2.83	-2.45	2.72	4.02	-1.28	4.02	2.66	6.85
150	400	-2.83	-2.70	2.72	3.50	-0.38	3.50	2.43	6.33
150	450	-2.06	-2.96	2.72	3.11	1.30	3.11	2.43	6.07
150	500	1.17	-3.22	1.95	4.40	3.89	4.40	2.93	7.62
150	550	1.43	-2.45	1.82	4.27	3.89	4.27	2.77	6.72
150	600	4.40	-1.28	1.04	2.98	4.66	4.66	1.87	5.94
200	50	-4.12	-3.35	2.34	0.01	-0.89	4.12	2.14	6.46
200	100	-2.83	-2.06	2.08	1.43	-1.02	2.83	1.88	4.91
200	150	-1.67	-0.64	2.98	1.56	0.14	2.98	1.40	4.65
200	200	-0.51	0.01	2.72	2.21	0.79	2.72	1.25	3.23
200	250	-1.28	0.01	4.02	2.46	-0.38	4.02	1.63	5.30
200	300	-2.19	-0.64	4.53	3.50	-0.77	4.53	2.32	6.72
200	350	-2.06	-1.54	4.53	2.72	1.43	4.53	2.46	6.59
200	400	-2.32	-2.32	4.14	4.02	2.34	4.14	3.03	6.46
200	450	-2.45	-2.32	3.50	5.18	3.50	5.18	3.39	7.62
200	500	-1.80	-2.19	3.63	4.92	3.63	4.92	3.23	7.11
200	550	0.27	-1.80	2.72	5.18	4.53	5.18	2.90	6.98
200	600	1.04	-1.02	2.98	3.50	3.50	3.50	2.41	4.52
250	50	-5.16	-2.19	2.46	-0.51	-0.51	5.16	2.16	7.62
250	100	-3.74	-2.32	2.21	1.56	-1.28	3.74	2.22	5.94
250	150	-2.70	-1.02	2.59	2.85	-0.89	2.85	2.01	5.56
250	200	-1.28	0.01	4.02	2.46	-0.38	4.02	1.63	5.30
250	250	-0.12	0.53	4.79	2.46	1.04	4.79	1.79	4.91
250	300	-0.89	0.27	4.92	4.40	-0.38	4.92	2.17	5.81
250	350	-1.54	0.01	4.53	5.18	0.66	5.18	2.38	6.72
250	400	-1.80	-0.64	4.27	6.73	2.46	6.73	3.18	8.53
250	450	-1.93	-1.15	4.53	6.73	4.02	6.73	3.67	8.66
250	500	-1.93	-1.28	4.66	5.70	5.31	5.70	3.77	7.62
250	550	-2.19	-0.77	4.02	5.57	4.92	5.57	3.49	7.75
250	600	1.17	-0.25	4.02	4.14	4.27	4.27	2.77	4.52

Figure 71. Load voltage second derivative